Long-term observations of Alaska Coastal Current in the northern Gulf of Alaska

Phyllis J. Stabeno[1*], Shaun Bell[1,2], Wei Cheng[1,2], Seth Danielson[3],
Nancy B. Kachel[1,2], Calvin W. Mordy[1,2],

[1] NOAA/Pacific Marine Environmental Laboratory
7600 Sand Point Way NE, Seattle, WA 98115-6349

[2] Joint Institute for the Study of the Atmosphere and Oceans
Box 354235, University of Washington, Seattle, WA 98195-4235

[3]Institute of Marine Science, University of Alaska, Fairbanks
112 O'Neill, Box 757220, Fairbanks, AK 99775-7220

[*]Corresponding author, phyllis.stabeno@noaa.gov, 206-526-6453

For submission to DSRII

September 2015

Contribution No. 4221 from NOAA/Pacific Marine Environmental Laboratory

Abstract

The Alaska Coastal Current is a continuous, well-defined system extending for ~1700 km along the coast of Alaska from Seward, Alaska to Samalga Pass in the Aleutian Islands. The currents in this region are examined using data collected at >20 mooring sites and from >400 satellite-tracked drifters. While not continuous, the mooring data span a 30 year period (1984 – 2014). Using current meter data collected at a dozen mooring sites spread over four lines (Seward, Gore Point, Kennedy and Stevenson Entrances, and the exit to Shelikof Strait) total transport was calculated. Transport was significantly correlated with alongshore winds, although the correlation at the Seward Line was weak. The largest mean transport in the Alaska Coastal Current occurred at Gore Point (1.4×10^6 m^3 s^{-1} in winter and 0.6×10^6 m^3 s^{-1} in summer), with the transport at the exit to Shelikof Strait (1.3×10^6 m^3 s^{-1} in winter and 0.6×10^6 m^3 s^{-1} in summer) only slightly less. The transport was modified at the Seward Line in late summer and fall by frontal undulations associated with strong river discharge that enters onto the shelf at that time of year. The interaction of the Alaska Coastal Current and tidal currents with shallow banks in the vicinity of Kodiak Archipeligo and in Kennedy-Stevenson Entrance results in mixing and prolonged primary production throughout the summer.

1. Introduction

The northern Gulf of Alaska (GOA) is an ecosystem dominated by advection, with the well-defined Alaska Coastal Current (ACC) transporting ~1 x 10^6 m^3 s^{-1} anti-clockwise along the coast (Royer, 1982; Stabeno et al., 2004; Weingartner et al., 2005). The ACC is driven by along-shore winds, with a hydrographic signature that is characterized by a low salinity core along the coast. This core results from river runoff, which is confined to the coast by downwelling-favorable winds. Along the shelf break, the slope and basin circulation is dominated by the cyclonic subarctic Alaska Gyre, which consists of the northward flowing Alaska Current, an eastern boundary current, and southwestward flowing Alaskan Stream, a western boundary current (Favorite and Ingraham, 1977).

While an ACC-type current exists along much of the North American coast from Vancouver Island to the arctic (Carmack, et al., in prep.), it is not a continuous feature (Stabeno et al., this issue). Some of these disruptions in the coastal flow are caused by deep submarine canyons, such as at Cross Sound, which cut across the entirety of the shelf. Others are caused by lack of downwelling favorable winds such as occurs between Cross Sound and Yakutat Bay (Stabeno et al., 2004, this issue). The focus of this manuscript is the region from the Kenai Peninsula to Samalga Pass. In this region, the ACC is largely continuous, although it can be interupted for short periods of time (days) by gap winds (Ladd et al., this issue) and upwelling favorable winds (Stabeno et al., 2004). In addition, it interacts with bathymetry (e.g. troughs, canyons, banks) which both divert water to the slope and introduce slope water onto the shelf (Mordy et al., this issue).

While from May to August there can be episodes of upwelling, downwelling dominates the northern GOA most of the year (Stabeno et al., 2004). In spite of this dominance of downwelling-

64 favorable winds, high productivity occurs in the northern coastal GOA. Nutrients are supplied to
65 the northern GOA shelf through several mechanisms including: advection, particularly associated
66 with canyons (Mordy et al., this issue); the relaxation of summer downwelling winds (Childers et
67 al., 2005; Ladd et al. 2005a); estuarine circulation (Stabeno et al., 2004); sediment resuspension;
68 river discharge (Royer, 2005); and, during winter, Ekman transport of surface water from the
69 central GOA basin onto the shelf (Stabeno et al., 2004). Collectively, these physical processes
70 support enhanced primary and secondary production during the spring and summer (Strom et al.,
71 2007; Coyle et al., 2012, 2013; Stabeno et al., 2004).
72 The GOA's pelagic production supports some of the nation's largest fisheries and vast
73 numbers of birds and mammals. The region around Kodiak Island (Fig. 1) is of particular
74 importance as a habitat for numerous economically and ecologically important fishes including
75 walleye pollock (Brodeur and Wilson, 1996), Pacific cod (Abookire, 2005), juvenile Pacific
76 halibut, arrowtooth flounder (Meuter and Norcross, 2002) and capelin (Doyle et al., 2002).
77 Kodiak Island is the site of major haul-out and rookery areas for Steller sea lions. Its nearshore
78 region and adjacent troughs support an abundance of juvenile and adult walleye pollock (Wilson,
79 2000; Hollowed et al., 2007).
80 Since the early 1980s, multiple papers have been published describing the ACC in the
81 northern GOA - its properties, seasonal variability and dynamics (e.g. Royer, 1981; Reed and
82 Schumacher, 1986; Schumacher et al., 1989; Kowalik et al., 1994; Stabeno et al., 1995, 2004;
83 Weingartner et al., 2005). Most of the papers concentrated on the long-term, hydrographic
84 transect at Seward and those in Shelikof Sea Valley and Strait. These hydrographic data were
85 often used to estimate the geostrophic velocity in the ACC. In 1984, the first arrays of moorings
86 measuring current velocity were deployed in Shelikof Strait and Sea Valley providing estimates

of total transport (Schumacher et al., 1989). In the 1990s mooring arrays measuring currents expanded to include Gore Point and Kennedy-Stevenson Entrances (Stabeno et al., 1995). With the deployment of a moored array of current meters on the Seward Line in 2001-2004, four lines existed at which transport could be calculated (Fig.1). These four cross-shelf mooring arrays were deployed as parts of several large ecosystem studies, including the US GLOBal Ocean ECosystems Dynamics (GLOBEC) Northern Gulf of Alaska program (2001-2005) and the more recent North Pacific Research Board (NPRB) Gulf of Alaska Integrated Ecosystem Research Project (2011-2014).

Most of the moorings in the northern GOA have been deployed intermittently. Only two of the mooring sites (Fig. 1) have been maintained nearly continuously for more than a decade – GAK1 (since 1998) and CB1 (since 1999). The GAK1 mooring records water properties at multiple depths, while CB1 measures both currents and water properties, but only near the bottom.

In this paper we integrate time series from 16 mooring sites (a total of 169 deployments distributed on four mooring array lines listed in Table 1 and in Fig. 2) and >400 satellite-tracked drifters, along with model simulations, to explore the temporal and spatial variability in the ACC from Seward to Cape Kekurnoi, including the differences between the cold "season" (October – April) and the warm "season" (May – September), spatial coherence and the relationship to winds. This large data set, together with other published results, permits the development of a schematic of the transports in ACC during the warm and cold seasons from Seward, Alaska to the eastern Aleutian Passes.

2 Methods

2.1 Winds

Reanalysis data was obtained from the North American Regional Reanalysis (NARR) and from the National Centers for Enironmental Prediction Reanalysis 2 (NCEPR2) for the North American Region. NARR uses the high resolution NCEP Eta model (~32 km grid size compared to NCEPR2's 2.5° grid) and includes additional assimilated parameters to improve the reanalyis product (Mesinger et al., 2004). NCEPR2 data is compared to the NARR output. Reanalysis estimates of winds are available at 3-hr intervals for NARR and 6-hr intervals for NCEPR2. Both data sets were binned and averaged into 12-hr intervals. The NCEPR2 and NARR data were provided by the NOAA/OAR/ESRL PSD, Boulder, Colorado, USA, from their web site at http://www.esrl.noaa.gov/psd/.

Wind velocity was measured on a series of surface moorings deployed on the Seward Line at GAK5 (2001 – 2004). Mooring winds were measured ~3 m above the ocean surface and are adjusted to the reanalysis height of 10 m assuming a power law wind profile and neutral stability (Hsu et al., 1994). All moored meteorological equipment (Coastal Environmental's WeatherPAK 2000 with an R/M Young Anemometer and Eppley PSP Radiometer) was prepared and data processed according manufacturers' specification. Data were collected hourly and averaged into two bins: 00:00-12:00 GMT and 12:00-24:00 GMT for comparison with reanalysis data.

Moorings were deployed in spring and replaced in late summer or early fall. While the spring-summer equipment functioned well, the anemometers generally failed in late fall due to the high wind speeds that occur each fall at the site. In winter 2003, the entire surface toroid was lost, although the oceanographic equipment was recovered from the sea floor in the spring.

2.2. Moorings

132 This paper focuses on currents and water column measurements (temperature, salinity)
133 made at 16 sites (Figs. 1 and 2) during the period from 1984 to 2014. Subsurface moorings were
134 all taut-wire, measuring temperature (SeaBird Electronics SBE-37, SBE39, and Aanderaa RCM-
135 9), salinity (SBE-37 and SeaCats), currents (RCM-7, RCM-9 and Teledyne RD Instruments
136 acoustic Doppler current profilers - ADCP). Most of the ADCP moorings consisted of a bottom
137 mounted, upward-looking 150 (prior to 2000), 300 or 75 kHz instruments (2000 – 2014). The
138 mooring at GAK4 consisted of two 300 kHz ADCPs, both at a depth of ~100 m, one upward-
139 looking and one downward-looking,
140 All moored oceanographic equipment was prepared and the data processed according to
141 manufacturers' specifications. Sampling on all instruments was at half-hourly or hourly intervals.
142 Temperature and salinity from the moored instruments were compared to available nearby
143 hydrographic casts for calibration.
144 Transport was calculated at each of the four lines (Shelikof Strait, Kennedy-Stevenson
145 Entrance, Gore Point and Seward lines; Fig. 1). Time series of the velocity component normal to
146 the mooring line were used to compute the transport through a section following Schumacher et
147 al. (1989). The normal component of velocity was low-pass filtered with a 35-hr, cosine-squared,
148 tapered Lanczos filter. This component of velocity at each current meter or ADCP bin was then
149 multiplied by the cross-sectional areas. The horizontal boundaries of cross sectional areas were
150 defined as the halfway line between moorings, or to the land, as appropriate. On the outer edge of
151 the mooring line at Gore Point and Seward, the edge was defined as the same half-distance as
152 between the outer mooring and its nearest more coastal neighbor. The vertical boundaries were
153 the surface, the bottom, or the halfway point between instruments, as appropriate. These time
154 series were then summed, providing a time series of transport perpendicular to the mooring line.

155 This method was successfully employed previously to obtain time series of transport in Shelikof
156 Strait (Stabeno et al., 1995), Gore Point (Stabeno et al., 1995) and the Alaskan Stream (Stabeno
157 Hristova, 2014).

158 Transport in Shelikof Strait (SS) were calculated using current measurements at SS1, SS2
159 and SS3 except from 15 January 1985 – 1 May 1985 and in 1989. During both periods, the
160 transport was calculatd using mooring arrays in the sea valley not at the exit of the Strait
161 (Schumcaher et al., 1989; Stabeno et al., 2004).

162 Unless otherwise noted, the current, temperature and salinity time series presented here
163 were low-pass filtered with a 35-hr, cosine-squared, tapered Lanczos filter to remove tidal and
164 higher-frequency variability. The time series were then re-sampled at 6-hour intervals.

165

166 2.3. Satellite-tracked drifters

167 Since 1986, >400 satellite-tracked drifters (drogue centered at ~40 m) have been deployed in
168 the North Pacific by investigators from the EcoFOCI program at Pacific Marine Environmental
169 Laboratory (www.ecofoci.noaa.gov/drifters/efoci_driftersIntro.shtml). During 1986-1988, “holey
170 sock” drogues were used, between 1987 and 1993, “tristar” drogues were employed, and since
171 1994 “holey sock” drogues have once again been used. At these northern latitudes, an average of
172 ~14 position fixes per day were obtained from Argos. Once the data were received from Argos,
173 the data were quality controlled. Data were deleted from the time series following loss of the
174 drogue. The resulting position time series were then linearly interpolated to hourly intervals.

175 Lagrangian velocities were determined by centered differences from the hourly drifter
176 positions. A low-pass filter (24 hour running mean) was applied to the drifter data. The methods
177 used in deriving mean velocities are described by Stabeno and Reed (1994). Data were gridded

into cells of 0.25° latitude by 0.5° longitude (~25 km x 25 km). In the northern GOA, the integral time scale for velocity (Kundu and Allen, 1976) was 1-3 days. Noting this, all measurements in a grid cell within a 3-day period were averaged together providing a set of independent estimate associated with that grid cell. Finally, if the derived scalar speed was less than the standard error, or there were fewer than five independent estimates, mean velocities were not considered sufficiently robust to be included. Lagrangian velocity is particularly useful in revealing spatial patterns of flow, but is not directly comparable to the Eulerian (from current meters) velocities.

2.4 Model description

The Regional Ocean Modeling System (ROMS) version 3.0 is a hydrostatic, primitive equation, generalized sigma-coordinate model. A full description of ROMS can be found in Haidvogel et al. (2000, 2008), Shchepetkin and McWilliams (1998, 2003, 2005), and references therein. ROMS has been implemented on a series of grids with increasing horizontal resolution in the North Pacific Ocean (Curchitser et al., 2005; Hermann et al., 2009a,b). The particular grid used for this study has 3-km horizontal resolution and covers the entire GOA (Cheng et al., 2012). It has 42 levels vertically. Vertical tracer and momentum mixing is parameterized using the K-profile parameterization scheme (Large et al., 1994), which includes both a surface and a bottom boundary layer (Durski et al., 2004). The ROMS grid is oriented such that its "eastern" and "northen" boundaries are against the land mass, while its "southern" (intersects coast at ~52°N) and "western" (intersects the Alaska Peninsula at ~164°W) boundaries are open, allowing entry and exit of the Alaskan Stream and the exit of ACC (see Fig. 1 in Cheng et al., 2012). Tracer and 3-D momentum fields from Simple Ocean Data Assimilation (SODA; Carton and Giese, 2008) at the open boundaries are treated with a radiative boundary condition with adaptive nudging as

described by Marchesiello et al. (2001). The Chapman scheme is used for sea surface height (Chapman, 1985), and the Flather scheme is used for barotropic velocities (Flather, 1976).

Additionally, tidal forcing obtained from Foreman et al. (2000) is applied at the open boundaries. Four diurnal (O1, Q1, P1, and K1) and four semidiurnal (N2, S2, K2, and M2) tidal constituents are used. ROMS is driven by sea surface heat and momentum fluxes calculated using bulk algorithms (Fairall et al., 1996) given the time dependent atmospheric forcing and modeled sea surface temperature (SST). The atmospheric forcing is taken from Version 2 forcing for Common Ocean-ice Reference Experiments (CORE2) (http://data1.gfdl.noaa.gov/nomads/forms/mom4/COREv2.html). Forcing variables include sub-daily surface winds, sea level pressure, surface air temperature and specific humidity, precipitation, and radiation fluxes. The model is also driven by monthly estimates of freshwater runoff along the Alaskan coast. The runoff forcing is constructed by combining the mean spatial pattern of global runoff in Dai and Trenberth (2002) with the spatially integrated monthly runoff estimates of Royer and Grosch (2007 and T. C. Royer, personal communication; note these include all major rivers in the GOA, as well as distributed sources). The runoff is applied as freshening of the topmost model layer near the coast. Total runoff along each segment of coastline is distributed using an exponential taper based on distance squared from the coastal point to the interior of the ocean, with an e-folding scale of 30 km.

ROMS was initialized on January 10, 2000 based on the SODA products, and the model was run continuously through October 2005. Daily, tidally-filtered averages were saved for subsequent analyses.

3. Results and discussion

224 3.1 Winds

225 NCEP's Reanalysis product Version 2 (NCEPR2; Kalnay et al., 1996) has long been the
226 standard for atmospheric forcing data in oceanographic studies, especially when few direct
227 observations are available. Previous studies have discussed the quality of the reanalyis as it
228 pertains to the northeast Pacific. The influence of topography is not well resolved around coastal
229 locations in the NCEPR2 Reanalysis data resulting in a need for caution when using coastal winds
230 (Ladd and Bond, 2002). This may be even more confounded by complex terrain, such as the steep
231 coastal mountains that occur along the coast in the GOA (Fig. 1). Here, terrain flows such as gap
232 winds have been observed (Ladd et al., this issue). In addition, the Shelikof Strait lies between
233 the mountains of the Alaska Peninsula and Kodiak Archepelago, which results in down gradient
234 winds in the Strait (Stabeno et al., 2004).

235 Since meteorological data collected on the moorings deployed on the Seward line in 2001 -
236 2004 were not assimilated into the reanalysis product, they serve as a useful independent measure
237 of reanalysis accuracy. Two years (2001 and 2003) of wind data collected at GAK5 are compared
238 to the corresponding NARR and NCEPR2 winds (Table 2). The region of interest is the northern
239 GOA near the Kenai Peninsula (Fig. 1). Data were collected during May – November 2001 and
240 mid April – mid September 2003. Using the nearest model gridpoint, the NARR comparison
241 location is to the southeast of the mooring location whereas the NCEPR2 comparison location is
242 to the northeast close to the coast. No interpolation was used to account for the variation in
243 locations. The NARR wind velocity components were consistently better correlated ($r^2 = 0.84 –$
244 0.91) to the winds measured at GAK5 than those from NCEPR2 winds ($r^2 = 0.71 – 0.81$). NARR
245 winds were also found to be stronger than the NCEPR2 winds, although both across-shore and

246 along-shore components from NARR were still ~15% weaker than the observed winds measured
247 at GAK5 (Fig 3).
248
249 3.2 Spatial patterns of flow derived from satellite-tracked drifters and moorings
250 Mean Lagrangian velocity was calculated for two periods: the warm season (May 10 –
251 September 15) and for the cold season (October 1 – April 25). Many of the drifters entered into
252 the large eddies found in the basin (Ladd et al., 2005b; 2007) and remained within them for
253 months. These trajectories can dominate the signal. For instance, if an eddy remains nearly
254 stationary for 90 days, which is not uncommon, and the drifter remains within the eddy for that
255 period, then that single event contributes 30 data points to the average overwhelming the derived
256 pattern of non-eddy currents. The mean velocities shown here have excluded trajectories of
257 drifters caught in an eddy from the analysis.
258 The large number of drifter trajectories provide information on the spatial patterns of flow
259 (Fig. 4). The best coverage occurs to the west of the Seward (Fig. 4c, 4d). In general, the
260 currents on the shelf were stronger in the winter than the summer, but many of the patterns were
261 similar in the two "seasons." On the shelf from Yakutat Bay to Kayak Island, drifters were
262 advected westward (Stabeno et al., this issue). Both the cold and warm seasons showed an
263 interruption of the coastal flow at Kayak Island (Fig. 4). Most of the drifters were transported off
264 the shelf onto the slope at Kayak Island, requiring the ACC to reform along the coast somewhere
265 east of Kayak Island. West of the island, the flow was weak near the coast, but on the outer shelf,
266 there was onshelf flow especially during "winter" (Fig. 4 a, b). The drifter composites showed
267 the ACC began to reform along Montague Island and is well formed at Seward. A similar pattern
268 is evident in model runs (see Figure 2 in Wang et al., 2014). Of the 8 drifters advected into the

vicinity of Hinchinbrook Entrance, only one entered Prince William Sound. Recent analysis of 40 years of hydrographic data suggests that the Prince William Sound flow field is likely subject to significant inter-seasonal and inter-annual variability (Musgrave et al., 2013). During winter, the strong downwelling favorable winds force surface water, including the Copper River plume, through Hinchinbrook Entrance, while during summer, with the relaxation of downwelling favorable winds, the more dense deeper water flows over the Hinchinbrook sill through into Prince William Sound (Niebauer, 1994).

West of Prince William Sound, the flow continued southwestward along the Kenai Peninsula, and then entered Shelikof Strait through Kennedy and/or Stevenson Entrance. Observations from earlier data sets indicate that ~75% of the ACC, measured at the exit of Shelikof Strait, leaves the shelf via the Shelikof Sea Valley (Schumacher et al., 1989), although onshelf flow is evident in current meter records between the Semidi Islands and Chirikof Island in both summer and winter. The remainder of the ACC continues along the peninsula eventually entering the Bering Sea through Unimak Pass and the other shallow Aleutian Passes east of 170°W (Ladd et al., 2005a; Stabeno et al. 2005; Stabeno and Hristova, 2014).

Onshelf flow is evident in Amatuli Trough and near Hinchinbrook Canyon, but only in the "winter." The influence of the other troughs (Chiniak, Stevenson and Barnabus Troughs) is not evident in the Lagrangian current patterns, because of the relatively large grid scale. Their influence, however, is evident in individual drifter trajectories (e.g. Figure 8 in Ladd et al., 2005b; Figure 10 in Stabeno et al., 2004).

The Alaskan Stream is clearly evident along the slope shoreward of the Aleutian Trench (Fig. 4 a, b). A well-defined Alaskan Stream appears to form at the mid-point along Kodiak Island. The satellite-tracked drifter trajectories revealed large numbers of mesoscale eddies at the

292 head of the gulf near Amatuli Trough (Ladd et al., 2007). Since data from drifters in eddies were
293 not included in this analysis, there are fewer data points in this region. The recurrence and
294 persistence of eddies in this region is indicative of a poorly formed Alaskan Stream. The Alaskan
295 Stream continues to strengthen as it moves westward, with the largest mean near surface speeds
296 occurring near 164°W (Stabeno and Hristova, 2014). It appears that the near surface flow in the
297 Alaskan Stream was stronger in the winter than summer (Fig. 4), which was also observed farther
298 west at ~170°W (Stabeno and Hristova, 2014).
299
300 3.3 Vertical structure and transport derived from moored current meters
301 The vertical structure of currents, derived from the measurements on the moorings, shows a
302 similar pattern of the ACC at each of the four lines (Figs. 5 and 6), with the strongest currents
303 near the surface along the coast. At all depths, the mean flow at Gore Point and Kennedy-
304 Stevenson Entrances was positive (toward the west or southwest) with no reversals, but there was
305 northeastward flow (negative) near the bottom and on the southern side of Shelikof Strait. Along
306 the Seward line, the ACC was strongest at GAK2 and GAK3, and weak at GAK4. The flow at
307 GAK5 was near zero and actually negative (eastward) in the summer, indicating that site was
308 outside the ACC. As expected, the flow in the winter at Gore Point, Shelikof Strait and Seward
309 (there is no winter data at Kennedy-Stevenson Entrances) was stronger than that during the
310 summer months (Figs. 5 and 6).
311 Mean transports were greatest at Gore Point, ranging from a seasonal average of 0.39 to 0.89
312 x 10^6 m^3 s^{-1} (average 0.58 x 10^6 m^3 s^{-1}) in the summer months to 1.30 - 1.50 x 10^6 m^3 s^{-1} (average
313 1.38 x 10^6 m^3 s^{-1}) in the winter (Table 1). Mean net transports were weaker at the exit to Shelikof
314 Strait, ranging from 0.06 - 0.57 x 10^6 m^3 s^{-1} (average 0.32 x 10^6 m^3 s^{-1}) in the summer months to

315 0.77 - 1.23 x 10^6 m^3 s^{-1} (average 0.98 x 10^6 m^3 s^{-1}) in the winter. The flow in Shelikof is more
316 complex, however, with northeastward inflow typically on southern side of the strait and the
317 southwestward flowing ACC occupying the remainder of the cross section of the strait. Within
318 Shelikof Strait, the inflow is entrained into the ACC. The average inflow is 0.26 x 10^6 m^3 s^{-1}, in
319 the summer and 0.30 x 10^6 m^3 s^{-1} in the winter, which is similar to the measured inflow between
320 Semidi Islands and Chirikov Island (Fig. 1) of 0.2 x 10^6 m^3 s^{-1} measured in 1984-1985, the single
321 year that there were moorings there. The ACC's average transport (the southwestward flow) is
322 0.55 x 10^6 m^3 s^{-1} in the summer months and 1.28 x 10^6 m^3 s^{-1} in the winter months, making the
323 transport at the exit to Shelikof Strait slightly less than that measured at Gore Point. The other
324 two lines (Kennedy-Stevenson Entrances and Seward) have far fewer occupations (Fig. 2), and
325 only one winter occupation; this more limited data set indicated weaker transport than that at
326 Gore Point.

327 The time series of transport were significantly (95% significance level) correlated to local
328 NARR winds (Table 1), although the weakest correlations consistently occurred between the
329 transport on the Seward Line and the NARR winds. Usually the winds led the transport by 12 or
330 18 hr (the inertial period is ~18 hr). In general, the transports at Shelikof Strait, Gore Point and
331 Kennedy-Stevenson were all well correlated and usually in phase (Table 3). In contrast, the
332 correlations between the transports measured at the Seward Line and the transports measured on
333 other lines were at best weakly correlated. This helps define a possible length scale for the along-
334 shore coherence of the flow. Interestingly, this scale is appreciably shorter than the dominant
335 atmospheric length scales, suggesting the importance of other processes in regulating local flow
336 variations. Possible causes of the weak correlations are discussed in Section 3.4.

There were sufficient occupations at Gore Point and the exit of Shelikof Strait to examine magnitude of seasonal transport fluctuations. To simplify the comparison between the transports at the exit of Shelikof and at Gore Point, we focus on the net transport at the exit Shelikof Strait, not the larger ACC transport there. In 1991, one of the times when there were measurements on both lines, the transport at Gore Point was typically greater than that at Shelikof Strait (Fig. 7a). The variations in transports were similar at the two sites, with high and low (or negative) flow events occurring in phase at the two lines. On multiple occasions, Shelikof Strait transport was northeastward (negative), while at Gore Point the flow weakened (in phase) but did not reverse, suggesting flow around the outer side of Kodiak Island. During periods of negative flow at the exit of Shelikof Strait, there was enhanced northeastward flow along north side of Kodiak Island (Fig. 7 b, c), forced by southwesterly winds.

All the time series of transport at Gore Point and Shelikof Strait show similar patterns of flow to those that were observed in 1991 (Fig. 8 a, b). Transport was stronger in the winter than summer, with maximum episodic events at Gore Point and in the net transport at Shelikof Strait exceeding 3 x 10^6 m^3 s^{-1}. Stronger events (>4.5 x 10^6 m^3 s^{-1}) occurred when just the ACC transport is considered (Fig. 8c). Throughout the year, although primarily in summer, there were periods of 1-3 days when the net transport in Shelikof was negative; this did not happen at Gore Point. Because of this, the transport time series at Gore Point exhibits lower variance than the net transport at Shelikof Strait. In contrast, the monthly mean transports (Fig. 8e) were consistently greater at Gore Point than the net transport at Shelikof Strait. The transport in the ACC (downstream) was also marginally weaker (except in January) than at Gore Point. Using mean transports derived from Table 1, 55% (0.32 x10^6 m^3 s^{-1}/ 0.58 x 10^6 m^3 s^{-1}) of the summer transport at Gore Point flowed down Shelikof Strait and 71% (0.98 x 10^6 m^3 s^{-1}/ 1.38 x 10^6 m^3 s^{-1}) of the

360 winter transport flowed down the strait. The remainder must have been diverted to the southeast
361 of Kodiak Island: 0.22 x 10^6 m^3 s^{-1} in summer and 0.40 x 10^6 m^3 s^{-1} in winter.
362 The seasonality of transport in Shelikof Strait is also reflected in the trajectories of the
363 satellite-tracked drifters (Fig. 9). In summer, approximately half the satellite-tracked drifters
364 transiting along the Kenai Peninsula bypassed Kennedy-Stevenson Entrances and moved along
365 the southeast coast of Afognak and Kodiak Islands. In winter, the stronger flow in Shelikof Strait
366 resulted in most of the drifters entering the strait through Kennedy or Stevenson Entrances. This
367 increase in the total percentage of drifters advected down Shelikof Strait resulted from the
368 increased number of drifters transiting through Stevenson Entrance (i.e., a broadening of the
369 ACC).
370
371 3.4 Instabilities in the ACC
372 Mysak et al. (1981) observed low-frequency fluctuations in the southwestwardly flowing
373 ACC in Shelikof Strait. At the northern end of the strait, waves appeared at periods of 2.0 – 3.5
374 days, while downstream, at the exit, periods were slightly longer, at 4.4 – 6.2 days. The
375 wavelength was ~74 km. They attributed these fluctuations to baroclinic instability. Similarly,
376 waves in the coastal plume were also evident along the coast from Copper River to Kenai
377 Peninsula (Fig. 10). The true color image shows sediment, likely originating in the Copper River
378 (Wang et al., 2014), delineating the wave pattern (wavelength ~ 20 km) along the coast,
379 especially east of the Seward line. Along the Kenai Peninsula, to the west of Seward, there was
380 little evidence of these waves along the coast. Model simulations of salinity at 5 m (Fig. 10c)
381 show a similar, albeit weaker, pattern of waves along the coast east of Seward.

382 These observed and modeled meanders are clearly evident in the near surface salinity time
383 series at GAK2 and GAK3; there was no evidence of these meanders in the salinity records at
384 Gore Point (GP32 and GP34). There was a similar freshening at GAK1 in August – December,
385 but the variability at frequencies of 2-8 days was not correlated with the variability at GAK2. In
386 2001, a series of 6 crests could be seen in the cross section of salinity extending ~50 km from the
387 coast (Fig. 11 a). The wave was not evident in temperature and appeared to be confined to the
388 upper ~80 m in salinity (Fig. 11 b, c). In the model the wave was less distinct - the salinity signal
389 was weaker and had a longer period. The weaker across-shelf gradient in the modeled salinity
390 was likely an artifact of how freshwater was introduced along the coast and enhanced diffusion in
391 the model. This weaker gradient would likely result in the longer period evident in model
392 simulation compared to the observations (Fig. 11 a vs. 11 d). The wave was also evident in the
393 currents at GAK2, and to a lesser extent at GAK3, and in the modeled velocity at 10 and 25 km. It
394 would not be expected, however, for the model to reproduce the exact timing of the instabilities.
395 These waves were evident each year at GAK2 and GAK3, beginning in July or August and
396 persisted into autumn, and sometimes into winter (e.g. 2013, Fig. 12). The signal was strongest at
397 ~2 d, but a significant increase in energy extended to ~4 d in 2001 and 2003. The timing of these
398 waves coincided with the seasonal increase in freshwater outflow from rivers, which occurs in
399 August (Royer, 1982; Weingartner et al., 2005).
400 These meanders are one possible explanation for the poor correlations between the transport
401 at Seward and those measured at the other mooring lines, and between the transport at Seward
402 and the along-shore winds (Tables 1 and 3). Such waves may cause enhanced flow near GAK4
403 (and thus an under-estimation of the calculated transport) or even a partial interruption in

404 transport. The lack of velocity measurements at GAK4 in 2001 – 2004 precluded examination of
405 this hypothesis.
406
407 3.5 Bottom salinity signal in long-term records
408 In addition to a well-defined surface flow, the ACC, together with flow in the canyons and
409 troughs, plays an important role in vertical and horizontal mixing of water (Mordy et al., this
410 issue). Stabeno et al. (2004) commented that the strong flow of the ACC through Kennedy
411 Entrance results in deep mixing, introducing salt (including nutrients) to surface waters and heat
412 to near bottom water. Two long-term moorings, one at GAK1 and the second (CB1) in a bay near
413 the Port of Kodiak on Kodiak Island provide insight into the impact of mixing on the bottom
414 temperature and salinity in the northern GOA. The bottom moorings are at similar depths - 250
415 m at GAK1 and 200 m at CB1.
416 The annual temperature and salinity cycles at the long-term moorings at Seward (GAK1) and
417 at the head of Chiniak Trough (CB1) are markedly different (Fig. 13 a, b). The weak annual
418 temperature signal at GAK1 has a maximum in early winter and a minimum in spring, while the
419 larger signal at CB1 has a maximum in September and a minimum in March, very similar to the
420 timing of the seasonal surface signal (Stabeno et al., 2004). That the temperature at CB1 is
421 approximately in phase with the near-surface ocean temperature indicates that strong surface-to-
422 bottom mixing occurs throughout the year. In contrast, at GAK1 heat is deeply mixed only in the
423 winter, when stratification weakens and winds intensify (Janout et al., 2010). Major mixing on the
424 shelf of the northern GOA likely occurs on the banks (Cheng et al., 2012; Mordy et al., this issue)
425 and in regions of strong currents (including tides) such as Kennedy Entrance (Stabeno et al.,
426 2004).

427 The stronger salinity signal was at GAK1, with lowest near-bottom salinities occurring in
428 March, which is indicative of downward mixing of surface water primarily during winter. Higher
429 salinities in summer were coincident with relaxation of downwelling, and the deep intrusion of
430 saltier water onto the shelf (Ladd et al., 2005a). The weaker salinity signal at CB1was freshest in
431 early September (in phase with freshening of the surface), supporting the conclusion derived from
432 the temperature time series that strong vertical mixing occurred throughout the year.
433 Even though the phase of the annual temperature signals differed markedly between these
434 two long-term deep measurements, the temperature anomalies (temperature time series minus the
435 annual signal in Fig. 13 b) appeared related at low frequency (Fig.13c). The monthly averaged
436 time series anomaly at the two sites are correlated at r = 0.65, with GAK1 lagging CB1 by two
437 months. Not unexpectedly, both monthly mean temperature anomalies, in turn, were well
438 correlated with the Pacific Decadal Oscillation (PDO), with the PDO signal leading the monthly
439 mean temperature anomaly at CB1 (GAK1) by 1 (4) months with a correlation of 0.52 (0.38).
440 That the monthly anomalies in temperature at CB1 lead those at GAK1 is a result of mixing of
441 warm surface waters to depth at CB1. Thus, the surface temperature signal arrives at depth first
442 at CB1 and later at GAK1.
443
444 3.6 Implications of mixing
445 A composite image of ocean color in August 2002 – 2011 (Fig. 14) shows higher
446 concentrations of chlorophyll-*a* during summer surrounding Kodiak Island relative to other shelf
447 waters in the GOA. On average, the highest chlorophyll concentrations appeared to be centered
448 over and near the shallow banks south and east of Kodiak Island and in Shelikof Strait, with
449 lower concentrations in the troughs and along the Kenai Peninsula, consistent with modeled

450 results (Coyle et al., 2012; Cheng et al., 2012). These persistent features of increased summer
451 chlorophyll concentrations can be interpreted as regions of higher primary production (Behrenfeld
452 and Falkowski, 1997), where new production was sustained throughout the summer. Note the
453 signals in upper Cook Inlet and in some coastal bays along the Alaska Peninsula are likely related
454 to supended sediment. To sustain new production, effective mechanisms of cross-shelf and/or
455 vertical exchange must be operative, introducing nutrient-rich water into the euphotic zone of the
456 shelf adjacent to Kodiak Island.

457 The high chlorophyll concentrations in Shelikof Strait are likely a result of the strong tidal
458 mixing in Kennedy Entrance, which vertically mixes the water column (Stabeno et al., 2004).
459 Nutrients are mixed into the euphotic zone throughout the summer, and that water is then
460 advected southwestward down Shelikof Striat where it supports a phytoplankton bloom. In
461 addition, some (~10%) of the drifters that entered Kennedy Entrance then exited through
462 Stevenson Entrance. This increase in nutrient availability in euphotic zone could contribute to the
463 higher chlorophyll concentrations to the south of Stevenson Entrance, although mixing on banks
464 are likely more important (Cheng, et al., 2012).

465 During summer, approximately ~38% of the water which flows past Gore Point entered
466 neither Kennedy nor Stevenson Entrance, but turned southward along the coast of Kodiak
467 Archepelago. During summer, the water at Gore Point was largely unmixed, but data collected in
468 Chiniak Trough indicated strong mixing occurs in the trough and over the banks to the southeast
469 of Afognak Island (Mordy et al., this issue). The salinity and temperature signals at CB1 also
470 suggest that strong mixing occured in this region. This mixing introduces nutrients into euphotic
471 zone which would support prolonged production throughout the summer on the shelf around

Kodiak Island. The record at GAK1 supports the premise that vertical mixing is weaker along the Kenai Peninsula, thus resulting in more limited summer production.

4. Summary and Conclusions

The ACC is marked by strong spatial and temporal variability. Transport varies seasonally, with the strongest flow in late fall and winter and the weakest in summer. The transports at Gore Point, Kennedy-Stevenson Entrances and the exit to Shelikof Strait are largely controlled by along-shore winds. Model results show that an increase in freshwater does not result in a significant increase in the transport of the ACC (Herman and Stabeno, 1996).

While winds largely control the transport of the ACC, freshwater input controls its vertical structure and is the major cause of the 2-6 day waves that occur both in Shelikof Strait and near Seward. These waves are likely one of the causes of the poor correlations between the transport at Seward and those at Gore Point, Kennedy-Stevenson and the exit to Shelikof Strait. Another cause may be the influence of gap winds, which have little impact on the transport at Seward, but can modify the transport at the Kennedy-Stevenson Entrances by as much 0.4×10^6 m^3 s^{-1} (Figure 11 in Ladd et al., this issue) and the other two lines by a lesser amount. While gap wind events persist for relatively short periods of time, they drive intense surface processes during those intervals. Finally, the complexity of the bathymetry downstream from the Seward can also influence the currents.

Vertical mixing plays an important role in summer in introducing nutrients into the euphotic zone and supporting prolonged summer production around Kodiak Island. Strong tidal mixing in Kennedy Entrance introduces the nutrients to the surface which are then advected southwestward down Shelikof Strait by the ACC, thereby supporting summer phytoplankton blooms in the strait. In contrast, the higher production to the south of Kodiak Island appears to be

related more to mixing over the banks and at their edges (Cheng et al., 2012; Mordy et al., this issue).

The largest transport in the ACC was measured at Gore Point. It varies seasonally, with mean winter transport at Gore Point ~1.4 x 10^6 m^3 s^{-1} and summer transport ~0.6 x 10^6 m^3 s^{-1}. Using this as the reference, a schematic of relative transports along the 1700-km pathway from Seward to the eastern Aleutian Passes can be derived (Fig. 15). The composite velocity vectors derived from the drifter trajectories (Fig. 4) shows the ACC beginning to reform along Montigue Island. This is supported by modeling work of Wang et al. (2014). The transport at Gore Point is the combined flow at Seward and the westward flow on the north side of Amatuli Trough which originated at the slope. This onshore flow is likely an improtant source for nutrients for the region around Kodiak Island. While approximately a third (38% in summer and 29% in winter) of the transport at Gore Point flows southward along the east coast of the Kodiak Archipeligo, its exact pathway is unclear (open arrows). The composite vectors from the drifter trajectories (Fig. 4) indicate weak offshore flow on the south side of Amatuli Trough and alongshore flow on the south side of the Kodiak Archipelago. Approximately two-thirds of the Gore Point transport flows down Shelikof Strait past Cape Kekurnoi. The inflow up the Shelikof Sea Valley introduces ~0.3 x 10^6 m^3 s^{-1} into Shelikof Strait. This is entrained into the ACC, increasing the total outflow to 0.9 x 10^6 m^3 s^{-1}, slightly less than the transport at Gore Point.

The remainder of current schematic (Fig. 15) is derived from previous research. After exiting Shelikof Strait ~75% of the ACC flows down the sea valley between Chirikof and Semidi Islands, while the remainder continues along the Alaska Peninsula eventually flowing between the Semidi Islands and Sutwik Island (Schumacher et al., 1989). There was only one year of data in that study, so the 75% - 25% ratio is used for both summer and winter. Individual drifter

518 trajectories (not shown) indicate that the flow along the Alaska Peninsula bifurcates east of the
519 Shumagin Islands (at 160°W) and rejoins to the west. The magnitude of flow through Unimak
520 Pass is 0.2 x 10^6 m^3 s^{-1} in summer and 0.4 x 10^6 m^3 s^{-1} in winter (Stabeno et al., in press), while
521 the flow through the other shallow passes west of Unimak Pass is weak (~0.1; Stabeno et al.,
522 2005; Stabeno and Hristova, 2014). To balance the flow through the Aleutian Passes
523 approximately a third of the flow exiting the sea valley needs to return to the shelf in the shallow
524 trough to the west of Shelikof Strait. Such a return flow is evident in the drifter composites (Fig.
525 4) and in individual drifter trajectories (not shown), but no moorings have deployed in that
526 location so estimates of transport are not available.
527 The reliability of the transports depicted in Fig. 15 varies by location. The estimates of
528 transport at Gore Point, the exit to Shelikof Strait and Unimak Pass all are derived from many
529 years of observations. At Seward and Kennedy-Stevenson Entrances the observations are
530 dominated by summer measurments. Probably the weakest estimates are derived from the single
531 year of data which determines the split of the ACC in Shelikof Sea Valley. While the estimate of
532 the magnitude of transport that flows southeast of Kodiak Archipelago is reliable, its pathways
533 are largely inferred from drifters which provide little information of magnitude of transport or the
534 flow in the bottom portion of the water column. Additional targeted measurements in the
535 Shelikof Sea Valley and to the southeast of Kodiak would be useful, but likely not change the
536 basic structure of this schematic.

537 **5. Acknowledgements**

538 We thank Sigrid Salo for processing the SeaWiFS composite image. Special thanks go to
539 W. Floering and C. Dewitt for deployment and recovery of the moorings, David Kachel for
540 processing much of the mooring and drifter track data and David Musgrave for providing the data

from GAK4. We thank the captains and crews of the NOAA Ships *Oscar Dyson* and *Miller Freeman*. SeaWIFS level 1A data were obtained from the Goddard Earth Sciences Distributed Active Archive center, which is under the auspices of the National Aeronautics and Space Administration. Files were processed using SeaDAS (SeaWiFS Data Analysis System which is maintained and distributed by the Goddard Space Flight Canter. Use of this data is in accord with the SeaWiFS Research data Use Terms and Conditions Agreement. This publication is partially funded by the Joint Institute for the Study of the Atmosphere and Ocean (JISAO) under NOAA cooperative Agreement No, NA17RJ1232. The research was generously supported by grant from the NPRB-sponsored GOAIERP (G83), US GLOBEC Program, and NOAA's North Pacific Climate Regimes and Ecosystem Productivity (NPCREP) and Fisheries Ocanography Coordinated Investigations programs. This is contribution #0838 to Ecosystems and Fisheries Oceanography Coordinated Investigations, xxxx to JISAO and xxx to GOAIERP.

6. References

Abookrie, A.A., Duffy-Anderson, J.T., Jump, C.M., 2005. Habitat associations and diet of young of the year Pacific cod near Kodiak Island, AK. Mar. Biol. 150, 713–726.

Behrenfeld, M.J., Falkowski, P.J., 1997. A consumer's guide to phytoplankton primary productivity models. Limnol Oceanogr. 42, 1479–1491.

Brodeur, R.D., Wilson, M.T., 1996. Review of distribution, ecology, and population dynamics of age-0 walleye pollock in the Gulf of Alaska. Fish. Oceanogr. 5(Supp. 1), 148–166.

Carton, J.A., Geise, B.S., 2008. A reanalysis of ocean climate using Simple Ocean Data Assimilation (SODA). Mon. Weather Rev. 136, 2999–3017, doi:10.1175/2007MWR1978.1.

Chapman, D.C., 1985. Numerical treatment of cross-shelf boundaries in a barotropic coastal ocean model. J. Phys. Oceanogr. 15, 1060–1075.

Cheng, W., Hermann, A.J., Coyle, K.O., Dobbins, E.L., Kachel, N.B., Stabeno, P.J., 2012. Macro- and micro-nutrient flux to a highly productive submarine bank in the Gulf of Alaska: A model-based analysis of daily and interannual variability. Prog. Oceanogr. 101, 63–77, doi:10.1016/j.pocean.2012.01.001.

Childers, A., Whitledge, T.E., Stockwell, D.A., 2005. Seasonal and interannual variability in the distribution of nutrients and chlorophyll-a across the Gulf of Alaska Alaska shelf: 1998–2000. Deep-Sea Res. II 52, 193–216, doi:10.1016/j.dsr2.2004.09.018.

Coyle, K.O., Cheng, W., Hinckley, S., Lessard, E.J., Whitledge, T., Hermann, A.J., Hedstrom, K., 2012. Model and field observations of effects of circulation on the timing and magnitude of nitrate utilization and production on the northern Gulf of Alaska shelf. Prog. Oceanogr. 103, 16–41.

576 Coyle, K.O., Gibson, G.A., Hedstrom, K., Hermann, A.J., Hopcroft, R.R., 2013. Zooplankton
577 biomass, advection and production on the northern Gulf of Alaska shelf from simulations
578 and field observations. J. Mar. Sys. 128, 185–207.
579 Curchitser, E.N., Haidvogel, D.B., Hermann, A.J., Dobbins, E.L., Powell, T.M., Kaplan, A.,
580 2005. Multi-scale modeling of the North Pacific Ocean I: Assessment and analysis of
581 simulated basin-scale variability (1996–2003). J. Geophys. Res. 110, C11021,
582 doi:10.1029/2005JC002902.
583 Dai, A., Trenberth, K.E., 2002. Estimates of freshwater discharge from continents: Latitudinal
584 and seasonal variations. J. Hydrometeor. 3, 660–687.
585 Doyle, M.J., Busby, M.S., Duffy-Anderson, J.T., Picquelle, S.J., Materese A.C., 2002. Early life
586 history of capelin in the northwest Gulf of Alaska: A historical perspective based on larval
587 collections, October 1977–March 1979. ICES J. Mar. Sci. 59, 997–1005.
588 Durski, S.M., Glenn, S.M., Haidvogel, D.B., 2004. Vertical mixing schemes in the coastal ocean:
589 Comparison of the level 2.5 Mellor-Yamada scheme with an enhanced version of the K
590 profile parameterization. J. Geophys. Res. 109, C01015. doi:10.1029/2002JC001702.
591 Fairall, C.W., Bradley, E.F., Rogers, D.P., Edson, J.B., Young, G.S., 1996. Bulk parameterization
592 of air-sea fluxes for Tropical Ocean-Global Atmosphere Coupled-Ocean Atmosphere
593 Response Experiment. J. Geophys. Res. 101(C2), 3747–3764, doi:10.1029/95JC03205.
594 Favorite, F., Ingraham Jr., W.J., 1977. On flow in the northwestern Gulf of Alaska, May 1972. J.
595 Oceanogr. Soc. Japan 33, 67–81.
596 Flather, R.A., 1976. A tidal model of the north-west European continental shelf. Mem. Soc. R.
597 Sci. Liege 10, 141–164.

598 Foreman, M.G.G., Crawford, W.R., Cherniawsky, J.Y., Henry, R.F., Tarbotton, M.R., 2000. A
599 high-resolution assimilating tidal model for the northeast Pacific Ocean. J. Geophys. Res.
600 105(C12), 28629–28651, doi:10.1029/1999JC000122.
601 Haidvogel, D.B., Arango, H.G., Hedstrom, K., Beckmann, A., Malanotte-Rizzoli, P.,
602 Shchepetkin, A.F., 2000. Model evaluation experiments in the North Atlantic Basin:
603 simulations in nonlinear terrain-following coordinates. Dyn. Atmos. Oceans 32, 239–281.
604 Haidvogel, D.B., Arango, H., Budgell, W.P., Cornuelle, B.D., Curchitser, E., Di Lorenzo, E.,
605 Fennel, K., Geyer, W.R., Hermann, A.J., Lanerolle, L., Levin, J., McWilliams, J.C., Miller,
606 A.J., Moore, A.M., Powell, T.M., Shchepetkin, A.F., Sherwood, C.R., Signell, R.P., Warner,
607 J.C., Wilkin, J., 2008. Ocean forecasting in terrain-following coordinates: Formulation and
608 skill assessment of the Regional Ocean Modeling System. J. Comput. Phys. 227, 3595–3624.
609 Hermann, A.J., Stabeno, P.J., 1996. An eddy-resolving model of circulation on the western Gulf
610 of Alaska shelf: 1. Model development and sensitivity analyses. J. Geophys. Res. 101, 1129–
611 1149.
612 Hermann, A.J., Curchitser, E.N., Haidvogel, D.B., Dobbins, E.L., 2009a. A comparison of remote
613 vs. local influence of El Niño on the coastal circulation of the northeast Pacific. Deep-Sea
614 Res. II 56, 2427–2443, doi:10.1016/j.dsr2.2009.02.005.
615 Hermann, A.J., Hinckley, S., Dobbins, E.L., Haidvogel, D.B., Bond, N.A., Mordy, C., Kachel, N.,
616 Stabeno, P.J., 2009b. Quantifying cross-shelf and vertical nutrient flux in the Gulf of Alaska
617 with a spatially nested, coupled biophysical model. Deep-Sea Res. II 56, 2474–2486.

618 Hollowed, A.B., Wilson, C.D., Stabeno, P.J., Salo, S.A., 2007. Effect of ocean conditions on the
619 cross-shelf distribution of walleye pollock (*Theragra chalcogramma*) and capelin (*Mallotus*
620 *villosus*). Fish. Oceanogr. 16, 142–154. doi:10.1111/j.1365-2419.2006.00418.x.
621 Hsu, S.A., Meindl, E.A., Gilhousen, D.B., 1994. Determining the power-law wind-profile
622 exponent under near-neutral stability conditions at sea. J. Appl. Meteor. 33, 757–765.
623 Janout, M.A., Weingartner, T.J., Royer, T.C., Danielson, S.L., 2010. On the nature of winter
624 cooling and the recent temperature shift on the northern Gulf of Alaska shelf. J. Geophys.
625 Res. 115, C05023, doi:10.1029/2009JC005774.
626 Kalnay, E., Kanamitsu, M., Kistler, R., Collins, W., Deaven, D., Gandin, L., Iredell, M., Saha, S.,
627 White, G., Woollen, J., Zhu, Y., Leetmaa, A., Reynolds, R., Chelliah, M., Ebisuzaki, W.,
628 Higgins, W., Janowiak, J., Mo, K.C., Ropelewski, C., Wang, J., Jenne, R., Joseph, D., 1996.
629 The NCEP/NCAR 40-Year Reanalysis Project. Bull. Amer. Meteor. Soc. 77, 437–471,
630 doi:10.1175/1520-0477(1996)077<0437:TNYRP>2.0.CO;2.
631 Kundu, P., Allen, J., 1976. Some three dimensional characteristics of low-frequency current
632 fluctuations near the Oregon coast. J. Phys. Oceanogr. 6, 181–199.
633 Ladd, C., Bond, N.A., 2002. Evaluation of the NCEP/NCAR reanalysis in the NE Pacific and the
634 Bering Sea. J. Geophys. Res. 107(C10), 3158, doi: 10.1029/2001JC001157.
635 Ladd, C., Stabeno, P.J., Cokelet, E.D., 2005a. A note on cross-shelf exchange in the northern Gulf
636 of Alaska. Deep-Sea Res. II 52, 667–679.
637 Ladd, C., Kachel, N.B., Mordy, C.W., 2005b. Observations from a Yakutat eddy in the northern
638 Gulf of Alaska. J. Geophys. Res. 110, C03003.
639 Ladd, C., Mordy, C.W., Kachel, N.B., Stabeno, P.J., 2007. Northern Gulf of Alaska eddies and
640 associated anomalies. Deep-Sea Res. I 54, 487–509.

641 Ladd, C., Cheng, W., Salo, S., 2015. Gap Winds near Kodiak Island, Alaska and effects on
642 regional oceanography. Deep-Sea Res. II, this issue.
643 Large, W., McWilliams, J., Doney, S., 1994. Oceanic vertical mixing: A review and a model with
644 a non-local boundary layer parameterization. Rev. Geophys. 32, 363–403.
645 Marchesiello, P., McWilliams, J.C., Shchepetkin, A.F., 2001. Open boundary conditions for long-
646 term integration of regional oceanic models. Ocean Model. 3, 1–20.
647 Mesinger, F., DiMego, G., Kalnay, E., Mitchell, K., Shafran, P.C., Ebisuzaki, W., Jovic, D.,
648 2006. North American regional reanalysis. Bull. Amer. Meteorol. Soc. 87(3), 343–360,
649 doi:10.1175/BAMS-87-3-343.
650 Meuter, F.J., Norcross, B.L., 2002. Spatial and temporal patterns in the demersal fish community
651 on the shelf and upper slope regions of the Gulf of Alaska. Fish. Bull. 100, 559–581.
652 Mordy, C.W., Kachel, N.B., Stabeno, P.J., 2015. Influence of canyons and troughs on the
653 northern Gulf of Alaska shelf. Deep-Sea Res. II, this issue.
654 Musgrave, D.L., Halverson, M.J., Pegau, S.W., 2013. Seasonal surface circulation, temperature,
655 and salinity in Prince William Sound, Alaska. Cont. Shelf Res. 53, 20–29,
656 doi:10.1016/j.csr.2012.12.001.
657 Mysak, L.A., Muench, R.D., Schumacher, J.D., 1981. Baroclinic instability in a downstream
658 varying channel: Shelikof Strait, Alaska. J. Phys. Oceanogr. 11, 950–969.
659 Reed, R.K., Schumacher, J.D., 1986. Physical oceanography. In: Hood, D.W., Zimmerman, S.T.
660 (Eds.), The Gulf of Alaska: Physical Environment and Biological Resources. U.S. Department
661 of Commerce and U.S. Department of the Interior, pp. 57–75.
662 Royer, T.C., 1981. Baroclinic transport in the Gulf of Alaska. Part II. Fresh water driven coastal
663 current. J. Mar. Res. 39, 251–266.

664 Royer, T.C., 1982. Coastal freshwater discharge in the northeast Pacific. J. Geophys. Res. 87(C3),
665 22017–22021, doi:10.1029/JC087iC03p2017.
666 Royer, T.C., Grosch, C.E., 2007. Update of freshwater discharge model for Gulf of Alaska, North
667 Pacific Research Board Final Report, NPRB Project 734, 12 pp.
668 Schumacher, J.D., Stabeno, P.J., Roach, A.T., 1989. Volume transport in the Alaska Coastal
669 Current. Cont. Shelf Res. 9, 1071–1083.
670 Shchepetkin, A.F., McWilliams, J.C., 1998. Quasi-monotone advection schemes based on explicit
671 locally adaptive dissipation. Mon. Weather Rev. 126, 1541–1580.
672 Shchepetkin, A.F., McWilliams, J.C., 2003. A method for computing horizontal pressure-gradient
673 force in an oceanic model with a nonaligned vertical coordinate. J. Geophys. Res. 108(C3),
674 3090, doi:10.1029/2001JC001047.
675 Shchepetkin, A.F., McWilliams, J.C., 2005. The regional oceanic modeling system (ROMS): A
676 split-explicit, free-surface, topography-following-coordinate oceanic model. Ocean Model. 9,
677 347–404, doi:10.1016/j.ocemod.2004.08.002.
678 Stabeno, P.J., Hristova, H.G., 2014. Observations of the Alaskan Stream near Samalga Pass and
679 its connection to the Bering Sea: 2001–2004. Deep-Sea Res. I 88, 30–46,
680 doi:10.1016/j.dsr.2014.03.002,.
681 Stabeno, P.J., Reed, R.K., 1994. Circulation in the Bering Sea basin observed by satellite-tracked
682 drifters: 1986–1993. J. Phys. Oceanogr. 24, 848–854.
683 Stabeno, P.J., Reed, R.K., Schumacher, J.D., 1995. The Alaska Coastal Current: Continuity of
684 transport and forcing. J. Geophys. Res. 100, 2477–2485.

685 Stabeno, P.J., Kachel, D.G., Kachel, N.B. Sullivan, M.E., 2005. Observations from moorings in
686 the Aleutian Passes: Temperature, salinity and transport. Fish. Oceanogr., 14(Suppl. 1), doi:
687 10.1111/j.1365-2419.2005.00362.x, 39–54.
688 Stabeno, P.J., Bond, N.A., Hermann, A.J., Kachel, N.B., Mordy, C.W., Overland, J.E., 2004.
689 Meteorology and oceanography of the northern Gulf of Alaska. Cont. Shelf Res. 24, 859–897.
690 Stabeno, P.J., Kachel, D.G., Kachel, N.B., Sullivan, M.E., 2005. Observations from moorings in
691 the Aleutian Passes: Temperature, salinity and transport. Fish. Oceanogr. 14(Suppl. 1), 39–54,
692 doi:10.1111/j.1365-2419.2005.00362.x.
693 Stabeno, P.J., Bond, N.A., Kachel, N.B., Ladd, C, Mordy, C.W., Strom, S.L., 2016a. Southeast
694 Alaska: Currents, mixing and chlorophyll-a. Deep-Sea Res. II, this issue.
695 Stabeno, P.J., Danielson, S., Kachel, D., Kachel, N.B., Mordy, C.W., 2016b. Currents and
696 transport on the eastern Bering Sea shelf. Deep-Sea Res. II, accepted.
697 Strom, S.L., Olson, M.B., Macri, E.L., Mordy, C.W., 2007. Cross-shelf gradients in
698 phytoplankton community structure, nutrient utilization, and growth rate in the coastal Gulf
699 of Alaska. Mar. Ecol. Prog. Ser. 328, 75–92.
700 Wang, Y., Xue, H., Chai, F., Chao, Y., Farrara, J., 2014. A model study of the Copper River
701 plume and its effects on the northern Gulf of Alaska. Ocean Dyn. 64, 241–258,
702 doi:10.1007/s10236-013-0684-3.
703 Weingartner, T.J., Danielson, S.L., Royer, T.C, 2005. Freshwater variability and predictability in
704 the Alaska Coastal Current. Deep-Sea Res. II 52, 169–191.
705 Wilson, M.T, 2000. Effects of year and region on the abundance and size of age-0 walleye
706 pollock, *Theragra chalcogramma*, in the western Gulf of Alaska, 1985–1988. Fish. Bull. 98,
707 823–834.
708

7. Figure Captions

Figure 1. Map of the coastal Gulf of Alaska from Kayak Island to the exit of Shelikof Strait. Mooring locations have names or numbers. The insert shows the primary hydrographic lines along the Kenai Peninsula. The hydrographic line at Cape Kekurnoi coincides with the moorings there and is referred to as Line 8. The star on the east side Kodiak is the long-term mooring site CB1, and the one on the Seward line is GAK1. The inset shows the Seward Line (GAK), and the Gore Point (GP), Kennedy-Stevenson (KE-SE), and Afognak-Portlock (AP) lines.

Figure 2. Time line of moorings on which currents were measured. The files are broken into warm period (May 10 – September 15), indicated in gray, and the cold period (October 1 – April 25), indicated in black. If there were more than 10 days in a warm or cold period the grid is colored. List of all moorings used and their positions are shown at the bottom. Temperature and salinity were measured on GAK1 (1998 –present) and CB1 (1999 – present) are included in the list, but not on the time line. The two to three letter codes in mooring names are: SS – Shelikof Strait; GP – Gore Point; GAK – the Seward Line; KE Kennedy Entrance; SV – Stevenson Entrance; and CB – Chiniak Trough. GAK1 and GAK4 were deployed by the University of Alaska, Fairbanks and the remainder by the Pacific Marine Environmental Laboratory.

Figure 3. Comparison between NARR and measured winds at GAK5 during summer deployment of 2003 (April-September) for (a) alongshore winds and (b) across-shore winds. R^2 values for the linear fist are shown in the top left corner of each plot. These correlations are greater than those with the NCEP2 winds (not shown).

732 Figure 4. Maps of currents at ~40 m derived from drifter trajectories for a) summer and b)
733 winter. The number of independent estimates for each vector is shown in c) summer and d)
734 winter.
735
736 Figure 5. Cross section of mean currents (cm s^{-1}) perpendicular to the plane of the moorings with
737 positive into the page (southwestward) for summer at a) the Seward line, b) Gore Point, c)
738 Kennedy and Stevenson Entrances and d) Shelikof Strait. The means were calculated from all
739 available data at the mooring locations indicated in Figure 2.
740
741 Figure 6. Cross section of mean currents (cm s^{-1}) perpendicular to the plane of the moorings with
742 positive into the page (southwestward) for winter at a) the Seward line, b) Gore Point, and c)
743 Shelikof Strait. The means were calculated from all available data at the mooring locations
744 indicated in Figure 2.
745
746 Figure 7. a) Time series of net transport at Shelikof Strait (blue) and Gore Point (red) for 1991.
747 Cross sectional veclocity (cm s^{-1}) at exit of Shelikof Strait for b) June 23 and c) July 2. Velocities
748 are perpendicular to the plane of the moorings with positive into the page (southwestward) and
749 negative out of the page (northeastward).
750
751 Figure 8. Time series of transport at a) Gore Point, b) net transport at Shelikof Strait, c) ACC
752 transport at Shelikof Strait and d) the upstream transport at Shelikof Strait exit. Each time series
753 is shown muted in the background and the red dots are the monthly averages. e) The annual
754 signal (average of the individual monthly averages) for Gore Point (green), net Shelikof Strait
755 (blue) and ACC Shelikof (red).

Figure 9. The fate of drifters entering the box bounded by the Gore Point and Kennedy-Stevenson lines (Figure 1-inset): passing through Kennedy Entrance (KE); Stevenson Entrance (SE); grounding out on rocks; passing through to Shelikof Strait and then reversing course (in and out); or bypassing the entrances as they are carried south around Kodiak Island. Two periods are considered: a) summer, b) winter. Each drifter is in one and only one category.

Figure 10. True color satellite images for a) August 22, 2001 and b) September 3, 2002. c) Modeled 5-m salinity on September 10, 2001. Triangles mark stations on the Seward Line.

Figure 11. a) Time series of observed near-surface salinity (15 – 20 m) across the Seward line in 2001. The vectors are daily currents (from low pass filtered time series). b) Observed vertical structure of temperature (blue fill) and salinity (red) contours centered on 9 September 0600 GMT and c) 12 September 1200 GMT. d) Modeled salinity at 5 m depth for the same time period.

Figure 12. Wavelet power spectrum of salinity at GAK2 from May 25 to end of record for each year a) 2001-02, b) 2002-03, c) 2003-04, d) summer 2004. "Scales" are comparable to Fourier time periods in days. Contour intervals were chosen such that the indicated percentage falls below the power level contoured (e. g. 25% of the data falls below the first level contoured). The thick contour denotes the 95% confidence level against a red noise spectrum and the grey region denotes the "cone of influence" where edge effects become important.

779 Figure 13. a) The annual near-bottom a) salinity and b) temperature CB1 at Chiniak Bay (200 m)
780 and GAK1 at Seward (250 m). c) Temperature anomalies (6-hourly time series minus the annual
781 temperature signals shown in b).
782
783 Figure 14. SeaWiFS chlorophyll averaged between June 1 and August 31 for 1998-2002 showing
784 the high, sustained productivity that takes place around Kodiak Island.
785
786 Figure 15. Composite map of transport in the various banches of the ACC from Kayak Island to
787 the Aleutian Islands. The hollow arrows are extrapolated pathways of the ACC. The thin green
788 lines indicate likely contributions to the ACC in the east and measured upstream flow in Shelikof
789 Strait. The highest mean transport was measured at Gore Point. The other squares indicate the
790 percent of transport at Gore Point (GP) that occurs on each branch. The magnitude of inflow in
791 Shelikof Strait is also given (green box). The transports at the exit to Shelikof Strait (SS),
792 Kennedy-Stevenson Entrances (K-S), south side of Kodiak Archipeligo (OK) and Seward (GAK)
793 are from this paper. The estimate of transport between Sutwik and the Semidi Islands (Sut) and
794 between the Semidi Islands and Chirikof Islands (SSV) are from Schumacher et al. (1989). The
795 flow through Unimak Pass (UP) is from Stabeno et al. (2016b, in press) and Aleutian Islands (AI)
796 continuation is estimated from Stabeno et al. (2005).
797
798
799
800

Table 1. Statistics on transport measured at the four GOA lines: Shelikof Strait, Kennedy-Stevenson Entrances, Gore Point and the Seward Line. The shaded area in the first column indicates the winter period. Correlations are with NARR winds, with a positive lag indicating that the winds lead the transport. For two periods (14 January – 12 July 1985, and 10 May – 15 July 1989) transport was calculated from moorings in Shelikof Sea Valley not at the exit to Shelikof Strait, so there is no upstream calculation made.

	Start Date	# of 6 hr points	Correlation	Lag (days)	95% Sig. Level	Mean Transport (10^6 m^3 s^{-1})
Shelikof Strait – 3 moorings						
	Aug. 27, 1984	75	0.67	0.50	0.37	0.31 (0.66)
	May 10, 1985	288	0.58	0.50	0.27	0.57
	May 10, 1989	256	0.49	0.50	0.21	0.38
	May 10, 1991	486	0.49	0.75	0.17	0.54 (0.82)
	May 10, 1996	510	0.47	0.50	0.18	0.06 (0.34)
	May 10, 1998	486	0.49	0.50	0.21	0.21 (0.47)
	May 15, 2001	486	0.48	0.75	0.18	0.29 (0.58)
	May 15, 2002	400	0.45	0.75	0.20	0.21 (0.44)
	May 10, 2003	460	0.47	0.25	0.18	0.42 (0.63)
	May 23, 2004	468	0.27	0.5	0.17	0.09 (0.39)
	May 10, 2005	512	0.45	1.00	0.19	0.39 (0.58)
	Oct. 1, 1984[+]	810 (416)	0.62	0.50	0.14	1.02 (1.32)
	Mar. 16, 1996	150	0.59	0.75	0.32	0.77 (1.06)
	Feb. 21, 1998	240	0.45	4.5	0.25	0.83 (1.18)
	Oct. 1, 2001	378	0.55	0.5	0.28	1.23 (1.55)
	Jan 17, 2002	384	0.37	0.5	0.17	0.88 (0.99)
	Mar. 3, 2003	200	0.65	0.50	0.36	1.12 (1.49)
	Oct.1, 2004	810	0.52	0.50	0.17	0.91 (1.25)
	Oct. 1, 2005	240	0.55	0.50	0.22	1.07 (1.40)
Kennedy-Stevenson – 2 moorings (3 in 1991)						
	May 10, 1991	512	0.54	0.75	0.15	0.43
	May 10, 2011	512	0.70	0.75	0.28	0.56
	May 10, 2013	512	0.38	0.75	0.16	0.21
Gore Point – 3 moorings (7 in 1991)						
	June 1, 1991	420	0.60	0.75	0.18	0.74
	May 10, 1994	504	0.60	0.50	0.19	0.62
	May 13, 2001	486	0.46	0.50	0.17	0.57
	May 28, 2002	432	0.44	0.75	0.18	0.39
	May 10, 2003	500	0.45	0.75	0.14	0.59
	May 10, 2004	324	0.63	0.75	0.24	0.41
	May 10, 2011	500	0.65	0.50	0.25	0.44
	May 10, 2013	504	0.41	0.50	0.15	0.89
	Oct. 1, 2001	400	0.42	0.75	0.23	1.50
	Oct. 1, 2002	810	0.43	0.75	0.12	1.30
	Oct. 1, 2003	810	0.46	0.75	0.13	1.31
	Oct. 1, 2013	360	0.45	0.75	0.15	1.39
Seward Line – 3 or 4 moorings						
	May 16, 2001	486	0.24	0.50	0.16	0.36
	May 28, 2002	447	0.19	0.50	0.14	0.49
	May 10, 2003	512	0.21	0.50	0.14	0.46
	May 10, 2004	326	0.21	0.50	0.16	0.35
	Oct. 1, 2001	160	0.31	2.0	0.23	0.81

801
802

803

804 Table 2. Comparison between the observed winds at GAK5 and the modeled NARR and

805 NCEPR2 winds. These are vector correlations, with the angle between the vectors indicated in

806 the 3rd and 5th columns.

807
808

	NARR		NCEP-R2	
Mooring (GAK5) Period sampled	Vector correlation	Angle (°)	Vector correlation	Angle (°)
2001 summer	0.84	0	0.71	-19
2001 fall	0.91	22	0.81	7
2003 summer	0.90	7	0.76	-15

809

810

Table 3. Correlations (r) and the maximum correlation (r-max) among transports at the four GOA lines, along with the lag in days (within 1.5 days) for r-max. The 95% signifcance level (signif.). Italics indicate the correlation is not significant.

	Shelikof Strait			Kennedy-Stevenson			Gore Point		
	r/r-max	signif (95%)	lag (d)	r/r-max	signif. (95%)	lag (d)	r/r-max	signif (95%)	lag (d)
Summer-1991	**11 Apr -1 Oct**			11 Apr -1 Oct					
KE&SE	0.81/0.81	0.23	0.00						
Gore Pt.	0.83/0.83	0.24	0.00	0.85/0.85	0.24	0.00			
Summer-2001	**10 May -15 Sep**						10 May -15 Sep		
Gore Pt.	0.62/0.62	0.22	0.00						
Seward	0.21/0.30	0.2	0.25				0.10/0.20	0.20	0.50
Summer-2002	**28 May- 25 Aug**						28 May- 15 Sep		
Gore Pt.	0.37/0.37	0.32	0.25						
Seward	0.15/0.17	0.2	0.50				*0.04/0.32*	*0.23*	*1.00*
Summer-2003	**Jul 26- 15 Sep**						Jul 26- 15 Sep		
Gore Pt.	0.72/0.72	0.29	0.00						
Seward	0.57/0.57	0.38	0.00				0.42/0.42	0.26	0.00
Summer-2004	**23 May- 30 July**						23 May- 30 July		
Gore Pt.	0.58/0.60	0.24	0.25						
Seward	*-0.12/0.00*	*0.18*	*1.50*				0.11/0.24	0.18	1.50
Summer-2011				01 May -5 Oct					
Gore Pt.				0.78/0.78	0.41	0.00			
Summer-2013				04 May -30 Sep					
Gore Pt.				0.63/0.64	0.28	0.25			
Winter 2001-2	1 Oct.'01- 4						1 Oct. '01-9		
Gore Pt.	0.42/0.50	0.5	0.50						
Seward	0.49/0.49	0.26	0.00				0.30/0.33	0.23	0.00
Winter 2001-2	1 Oct. '01-9						1 Oct. '01-9		
Gore Pt.	0.50/0.52	0.31	0.25						
Seward	0.49/0.49	0.26	0.00				0.31/0.36	0.22	0.25
Winter 2003-4	1 Oct '03- 12 April								
Gore Pt.	0.61/0.61	0.19	0.00						

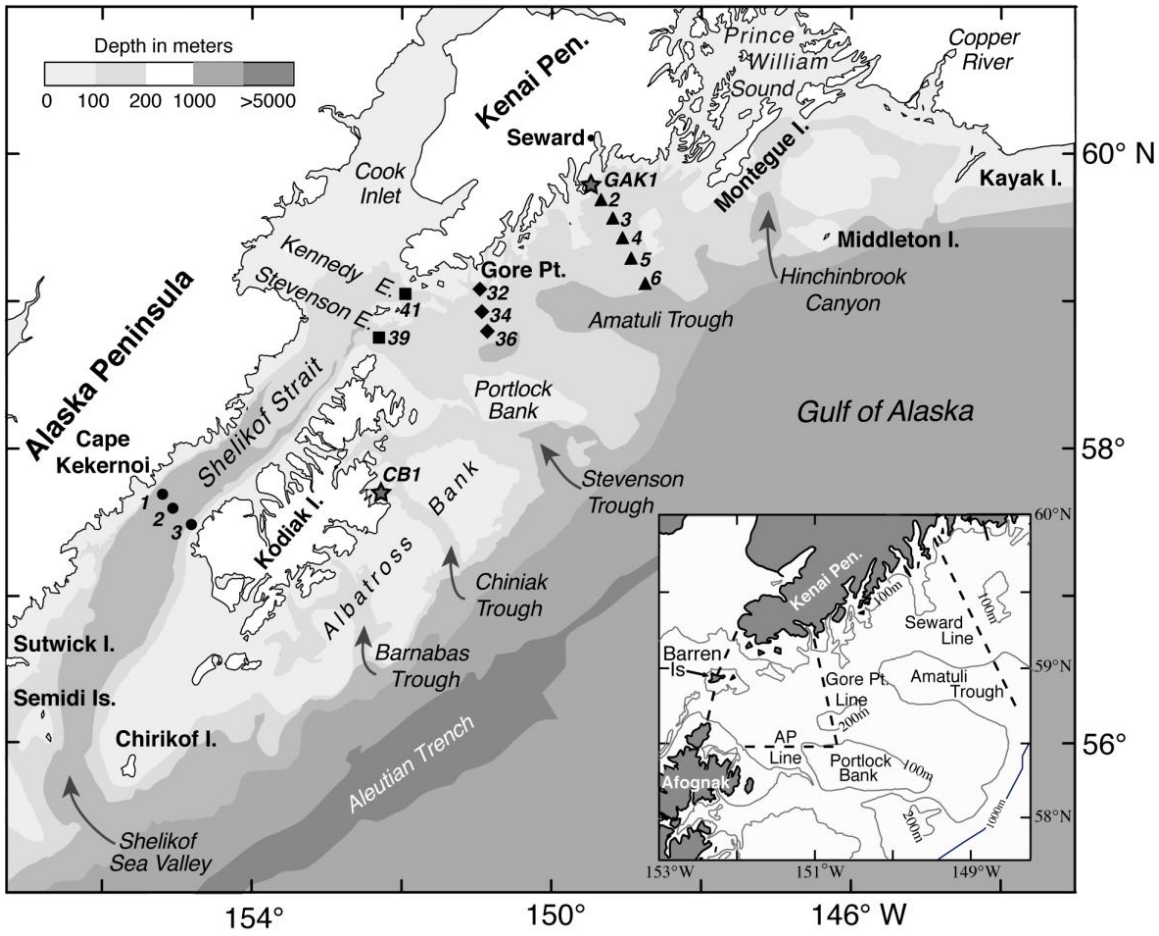

Figure 1. Map of the coastal Gulf of Alaska from Kayak Island to the exit of Shelikof Strait. Mooring locations have names or numbers. The insert shows the primary hydrographic lines along the Kenai Peninsula. The hydrographic line at Cape Kekurnoi coincides with the moorings there and is referred to as Line 8. The star on the east side Kodiak is the long-term mooring site CB1, and the one on the Seward line is GAK1. The inset shows the Seward Line (GAK), and the Gore Point (GP), Kennedy-Stevenson (KE-SE), and Afognak-Portlock (AP) lines.

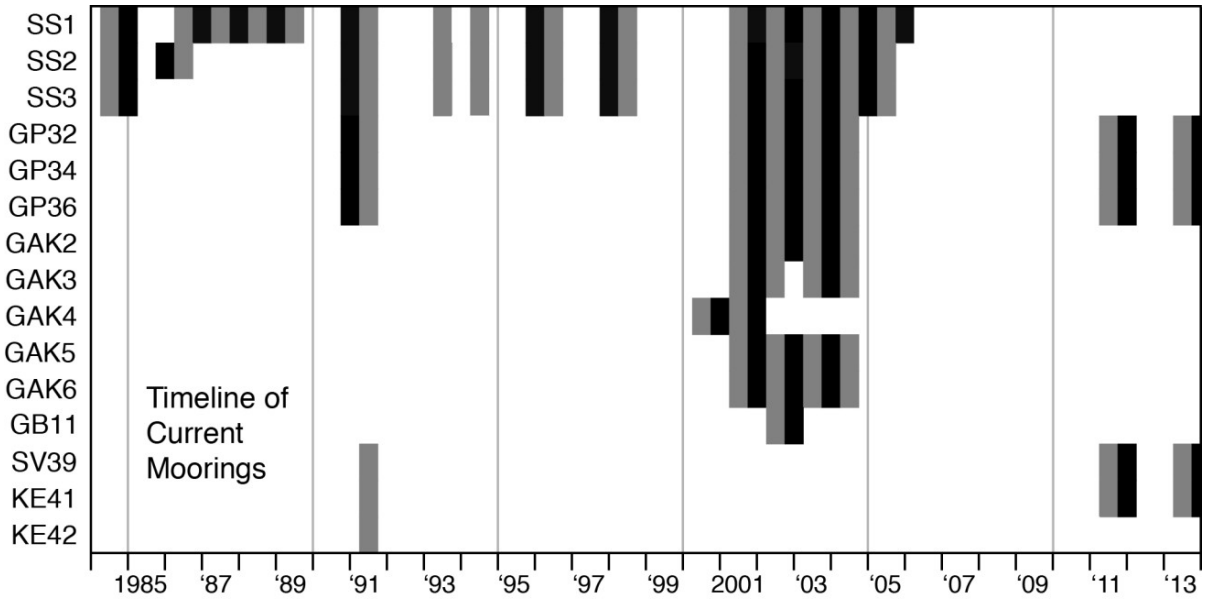

SS1: 57° 41.3', 155° 13'	SS2: 57° 37', 155° 4'	SS3: 57° 30', 154° 48'
GP32: 59° 6.0', 150° 59'	GP34: 58° 57', 150° 57'	GP36: 58° 49', 150° 53'
GAK1: 59° 50.7', 149° 28'	GAK2: 59° 6', 149° 22'	GAK3: 59° 43', 149° 12'
GAK4: 59° 24.6', 149°24.6'	GAK5: 59° 17', 148° 57'	GAK6: 59° 8', 148° 47'
KE41: 59° 16', 151° 51.7'	KE42: 58° 59.7', 151° 55.7'	SV39: 58° 45.9', 152° 14'
	CB1: 57° 43.2', 152° 17.4'	

Figure 2. Time line of moorings on which currents were measured. The files are broken into warm period (May 10 – September 15), indicated in gray, and the cold period (October 1 – April 25), indicated in black. If there were more than 10 days in a warm or cold period the grid is colored. List of all moorings used and their positions are shown at the bottom. Temperature and salinity were measured on GAK1 (1998 –present) and CB1 (1999 – present) are included in the list, but not on the time line. The two to three letter codes in mooring names are: SS – Shelikof Strait; GP – Gore Point; GAK – the Seward Line; KE Kennedy Entrance; SV – Stevenson Entrance; and CB – Chiniak Trough. GAK1 and GAK4 were deployed by the University of Alaska, Fairbanks and the remainder by the Pacific Marine Environmental Laboratory.

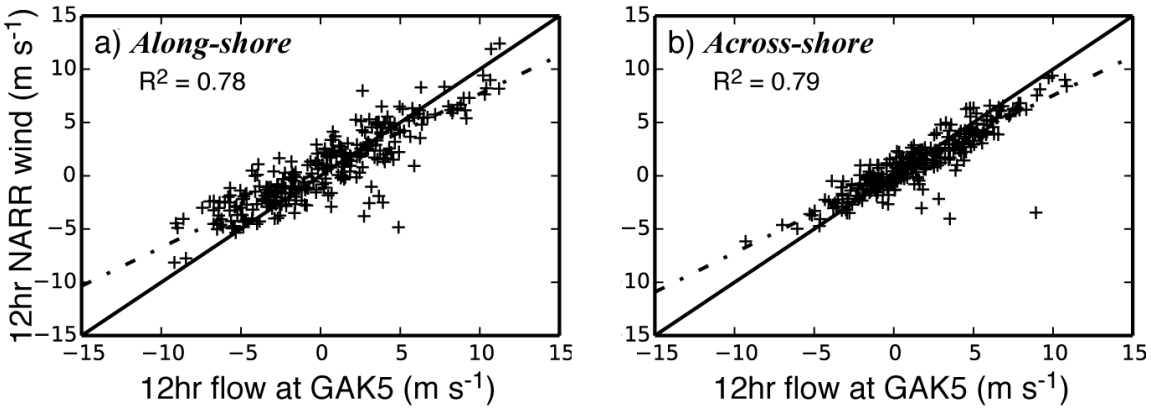

Figure 3. Comparison between NARR and measured winds at GAK5 during summer deployment of 2003 (April-September) for (a) alongshore winds and (b) across-shore winds. R^2 values for the linear fist are shown in the top left corner of each plot. These correlations are greater than those with the NCEP2 winds (not shown).

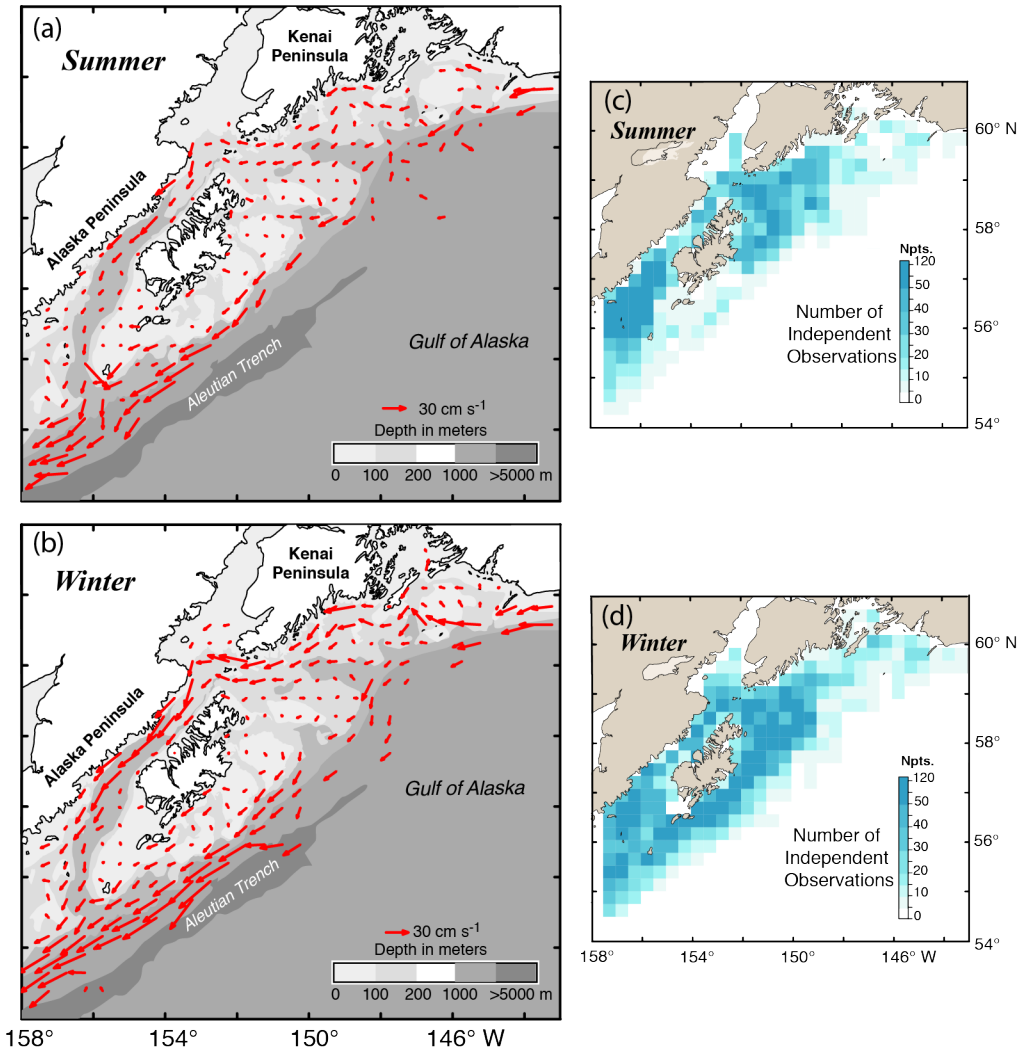

Figure 4. Maps of currents at ~40 m derived from drifter trajectories for a) summer and b) winter. The number of independent estimates for each vector is shown in c) summer and d) winter.

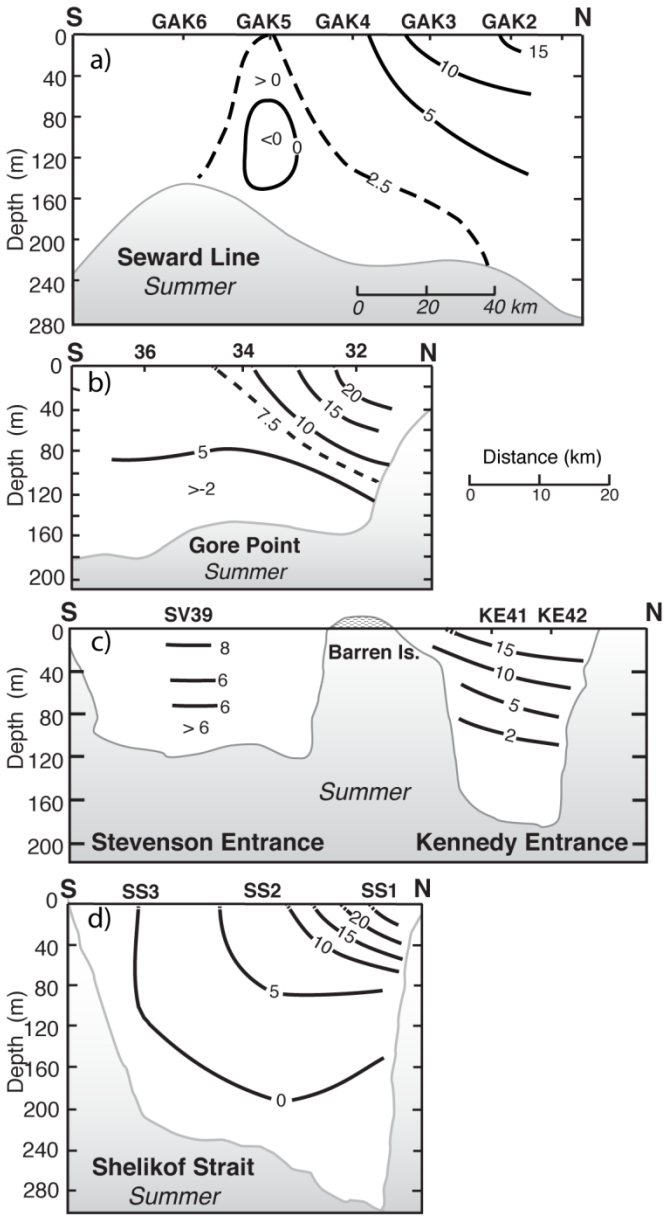

Figure 5. Cross section of mean currents (cm s^{-1}) perpendicular to the plane of the moorings with positive into the page (southwestward) for summer at a) the Seward line, b) Gore Point, c) Kennedy and Stevenson Entrances and d) Shelikof Strait. The means were calculated from all available data at the mooring locations indicated in Figure 2.

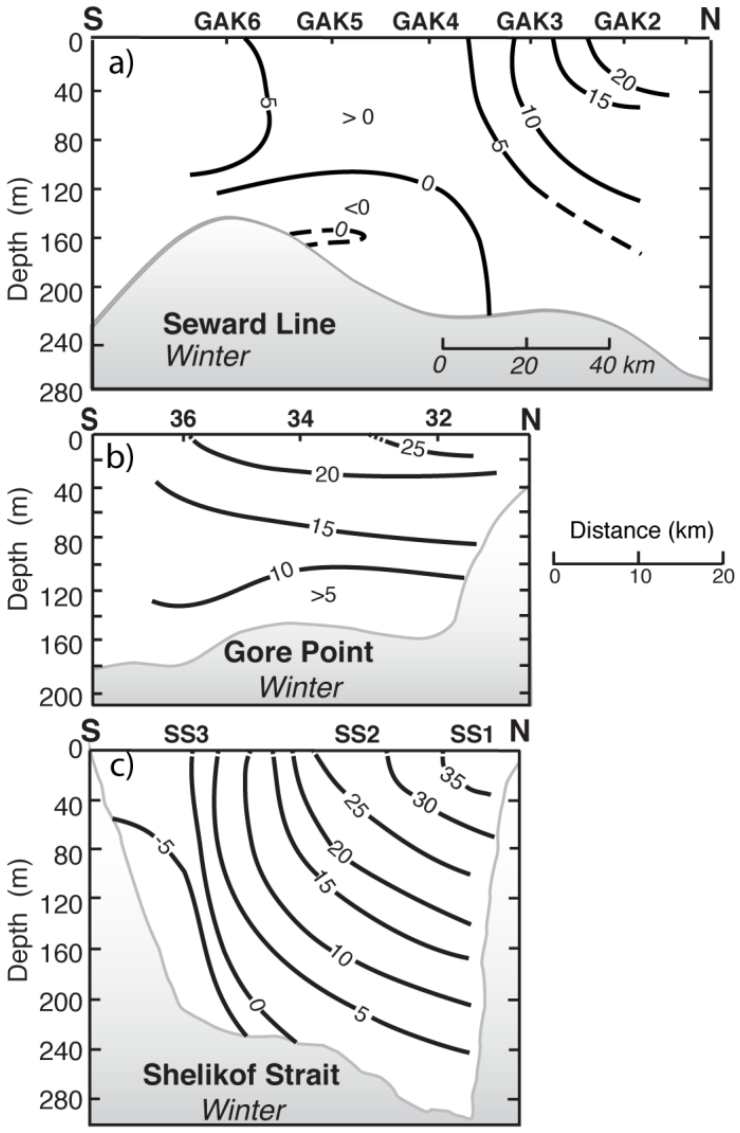

Figure 6. Cross section of mean currents (cm s^{-1}) perpendicular to the plane of the moorings with positive into the page (southwestward) for winter at a) the Seward line, b) Gore Point, and c) Shelikof Strait. The means were calculated from all available data at the mooring locations indicated in Figure 2.

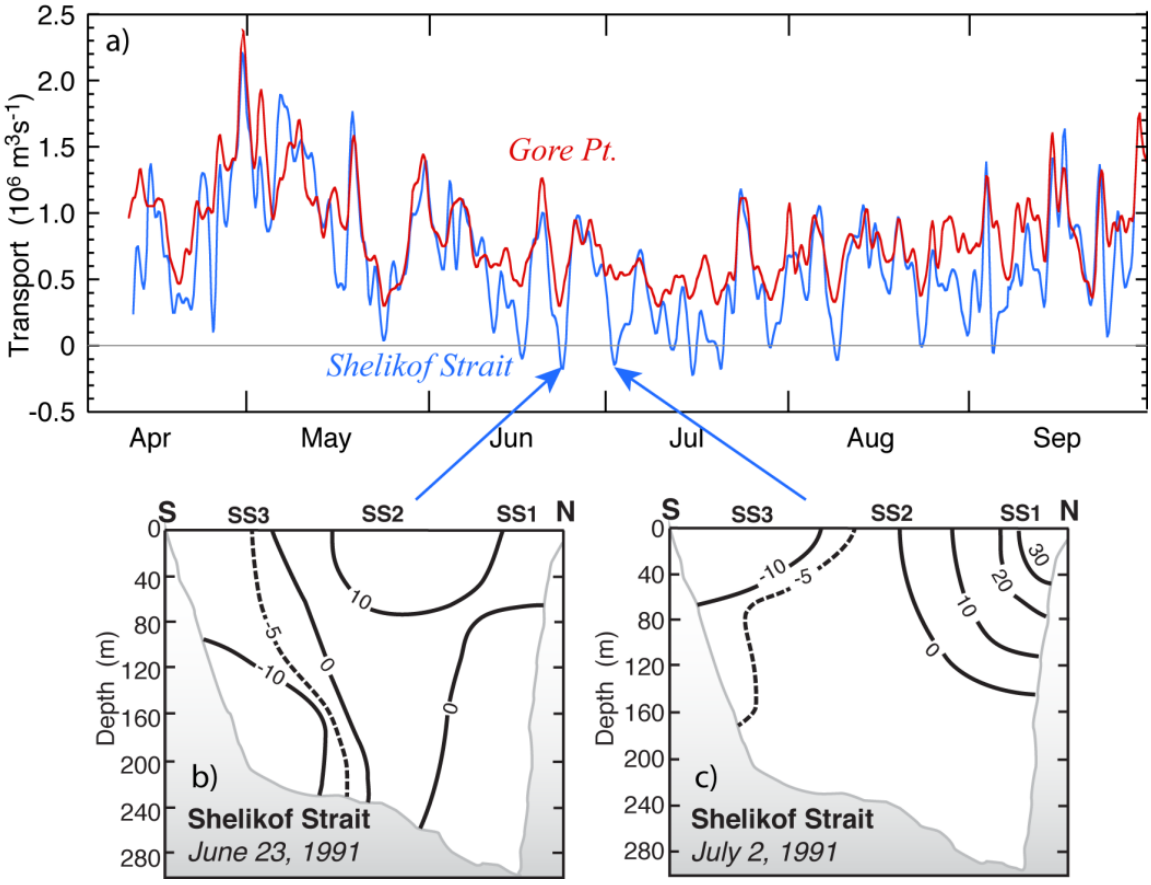

Figure 7. a) Time series of net transport at Shelikof Strait (blue) and Gore Point (red) for 1991. Cross sectional veclocity (cm s^{-1}) at exit of Shelikof Strait for b) June 23 and c) July 2. Velocities are perpendicular to the plane of the moorings with positive into the page (southwestward) and negative out of the page (northeastward).

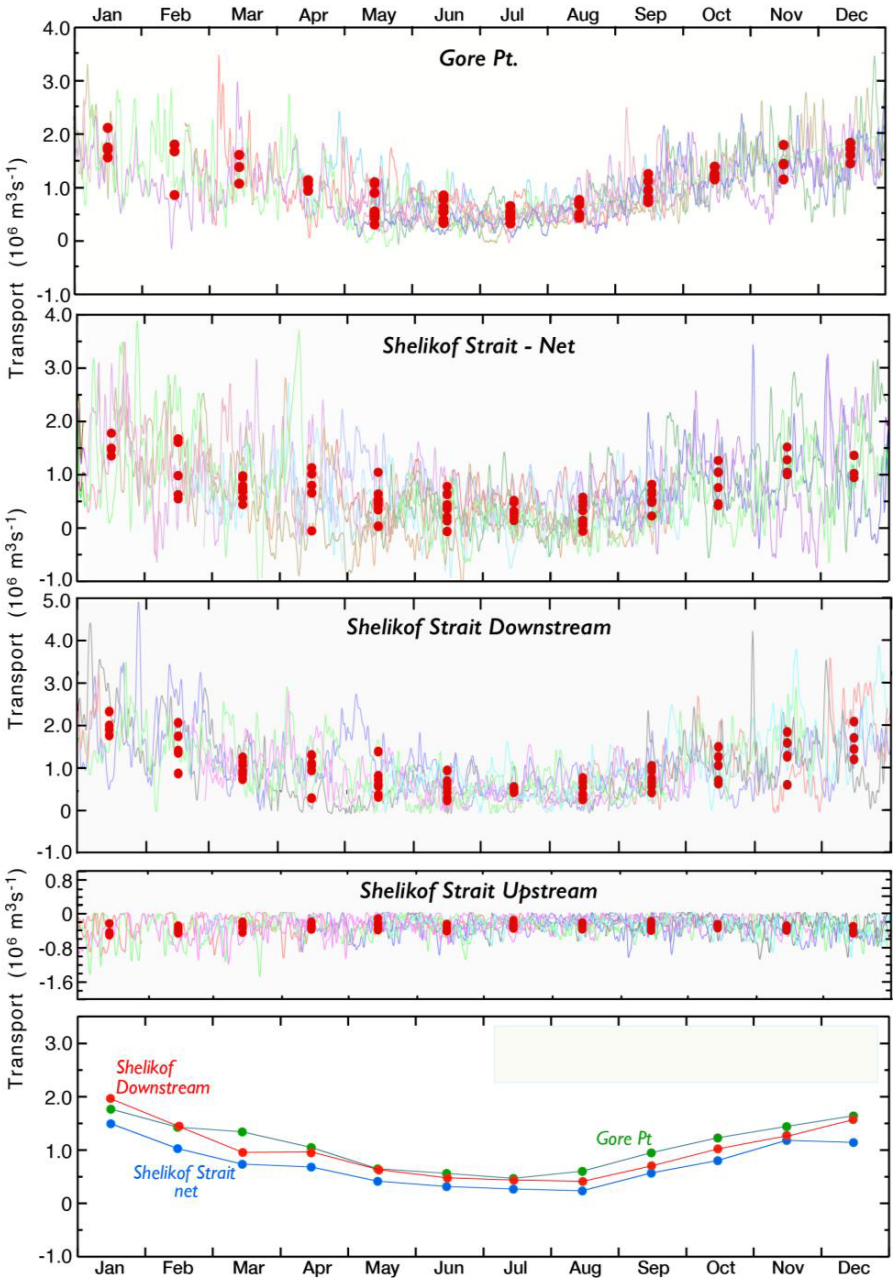

Figure 8. Time series of transport at a) Gore Point, b) net transport at Shelikof Strait, c) ACC transport at Shelikof Strait and d) the upstream transport at Shelikof Strait exit. Each time series is shown muted in the background and the red dots are the monthly averages. e) The annual signal (average of the individual monthly averages) for Gore Point (green), net Shelikof Strait (blue) and ACC Shelikof (red).

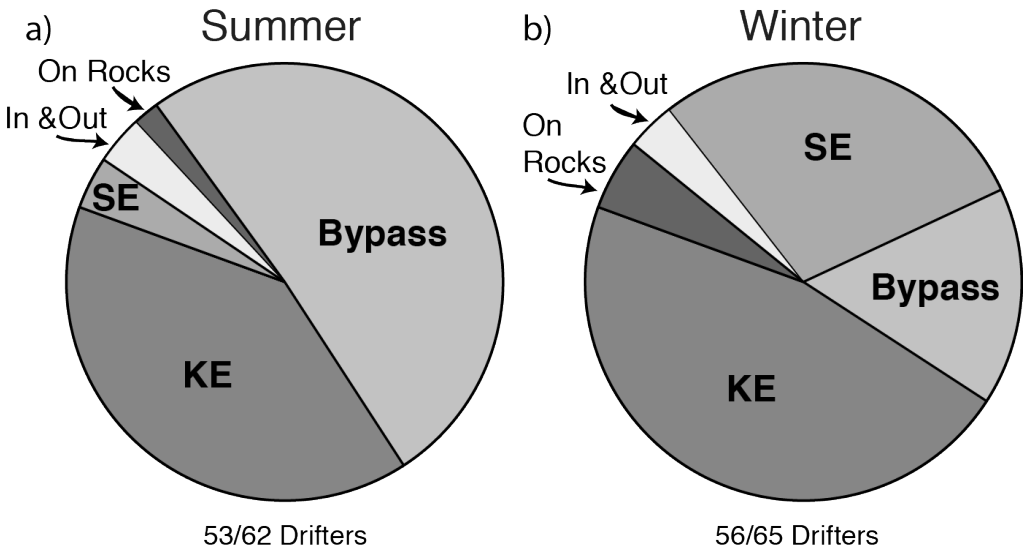

Figure 9. The fate of drifters entering the box bounded by the Gore Point and Kennedy-Stevenson lines (Figure 1-inset): passing through Kennedy Entrance (KE); Stevenson Entrance (SE); grounding out on rocks; passing through to Shelikof Strait and then reversing course (in and out); or bypassing the entrances as they are carried south around Kodiak Island. Two periods are considered: a) summer, b) winter. Each drifter is in one and only one category.

a)

b)

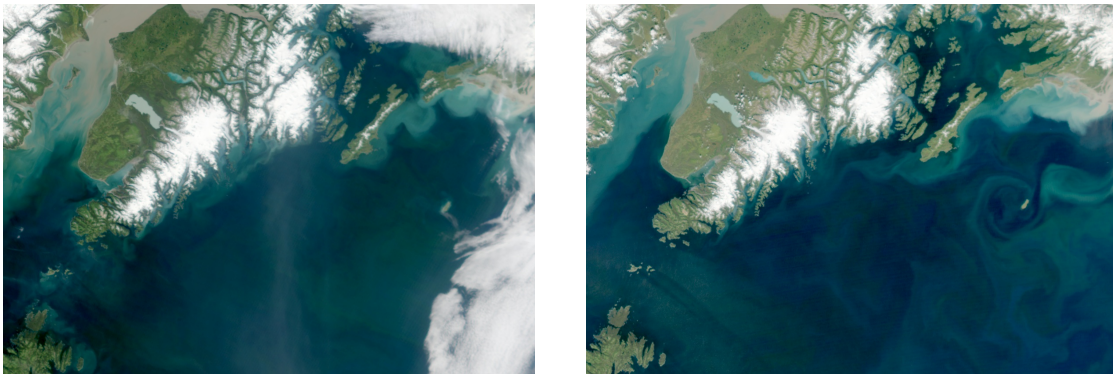

c)

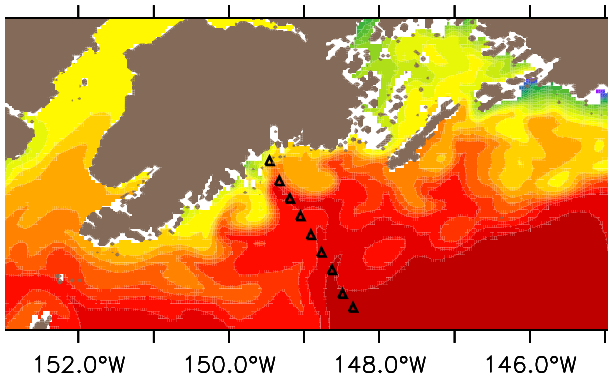

Figure 10. True color satellite images for a) August 22, 2001 and b) September 3, 2002. c) Modeled 5-m salinity on September 10, 2001. Triangles mark stations on the Seward Line.

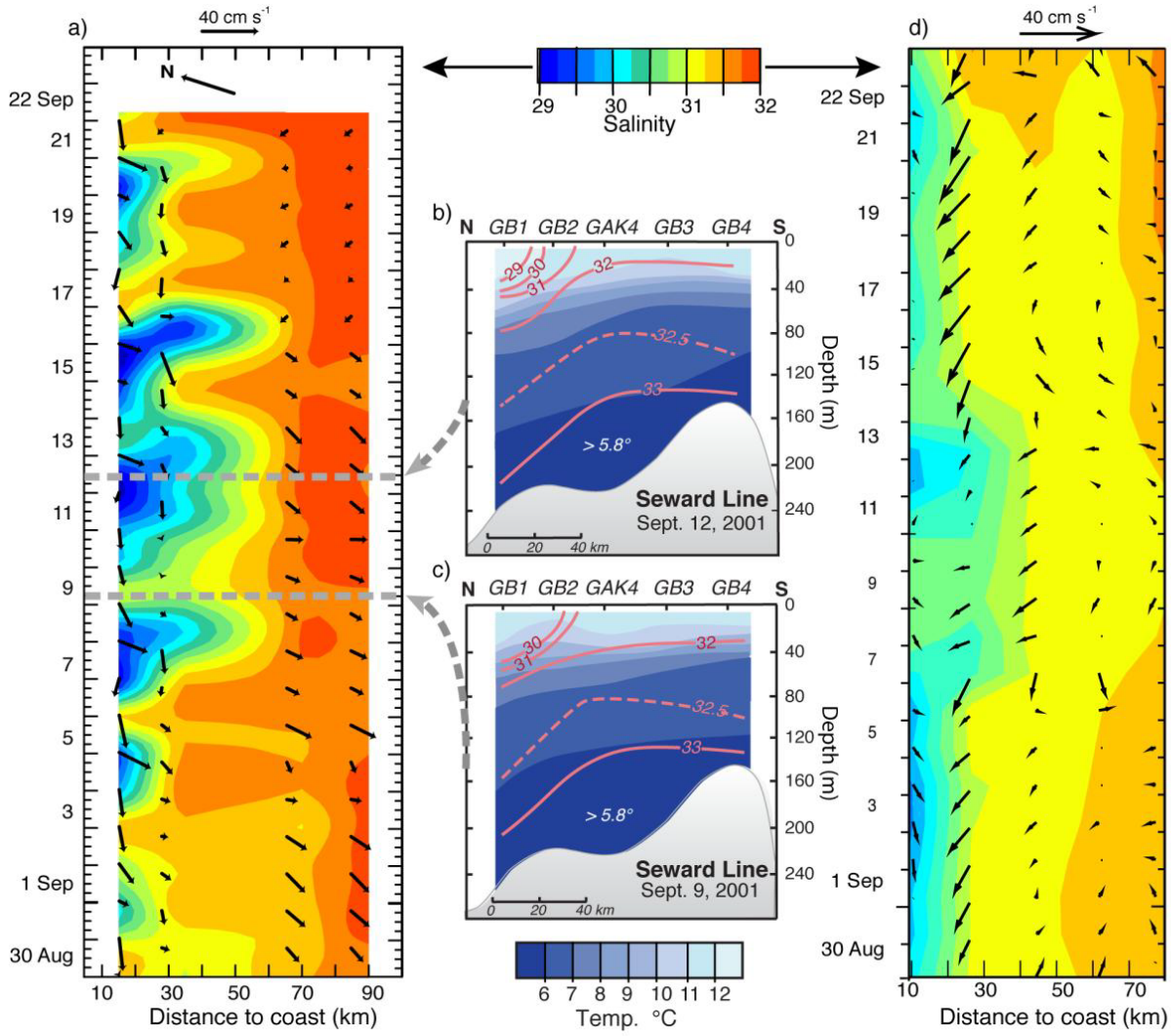

Figure 11. a) Time series of observed near-surface salinity (15 – 20 m) across the Seward line in 2001. The vectors are daily currents (from low-pass filtered time series). b) Observed vertical structure of temperature (blue fill) and salinity (red) contours centered on 9 September 0600 GMT and c) 12 September 1200 GMT. d) Modeled salinity at 5 m depth for the same time period.

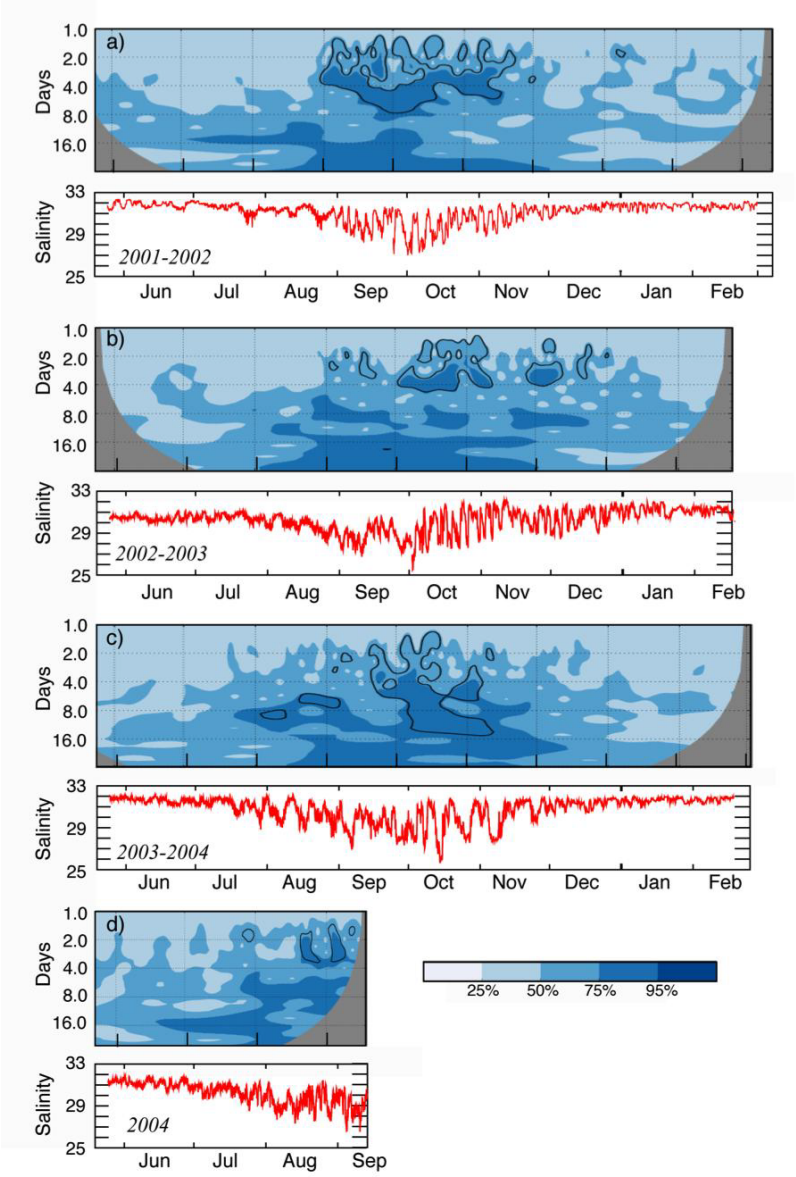

Figure 12. Wavelet power spectrum of salinity at GAK2 from May 25 to end of record for each year a) 2001-02, b) 2002-03, c) 2003-04, d) summer 2004. "Scales" are comparable to Fourier time periods in days. Contour intervals were chosen such that the indicated percentage falls below the power level contoured (e. g. 25% of the data falls below the first level contoured). The thick contour denotes the 95% confidence level against a red noise spectrum and the grey region denotes the "cone of influence" where edge effects become important.

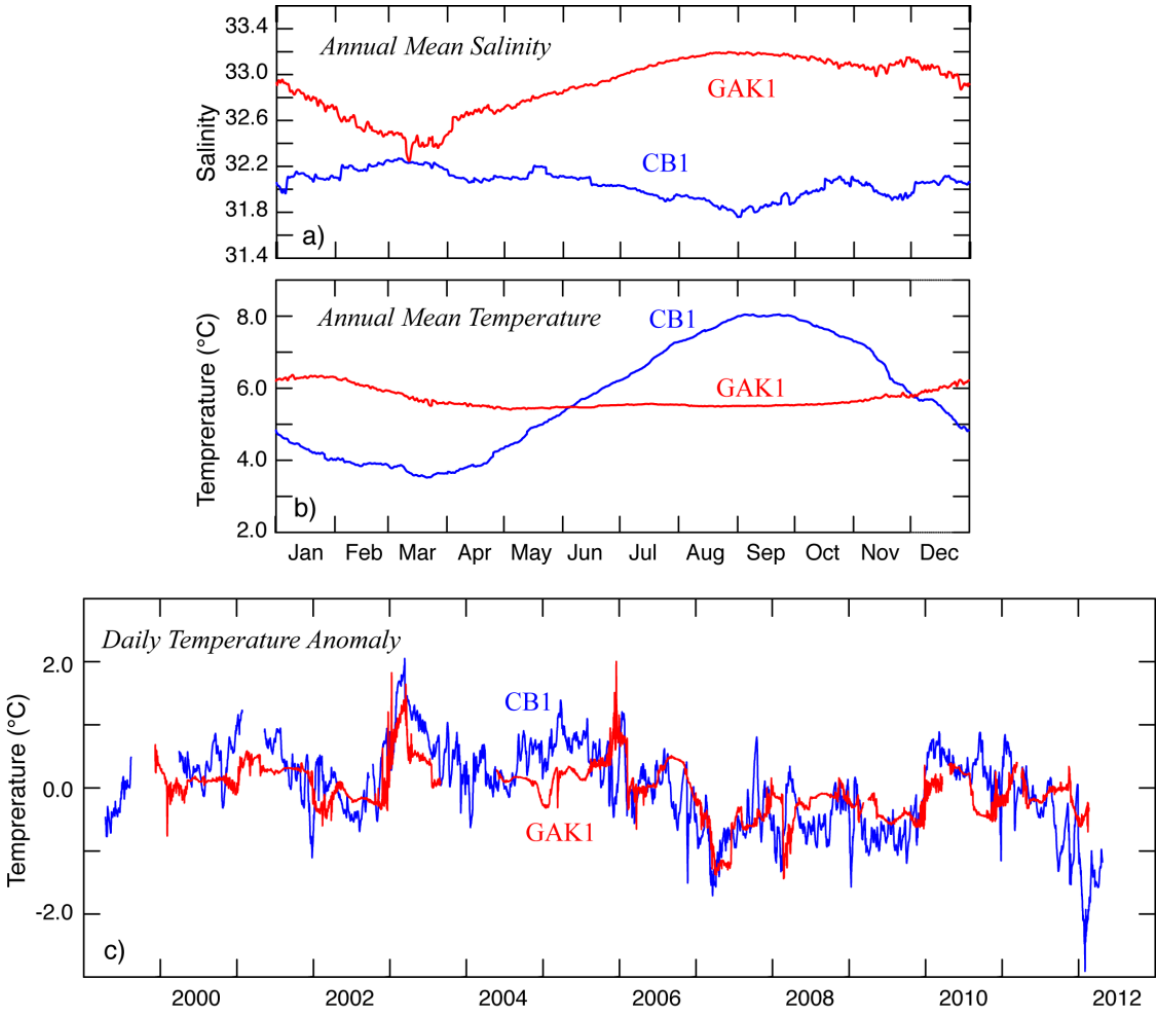

Figure 13. a) The annual near-bottom a) salinity and b) temperature CB1 at Chiniak Bay (200 m) and GAK1 at Seward (250 m). c) Temperature anomalies (6-hourly time series minus the annual temperature signals shown in b).

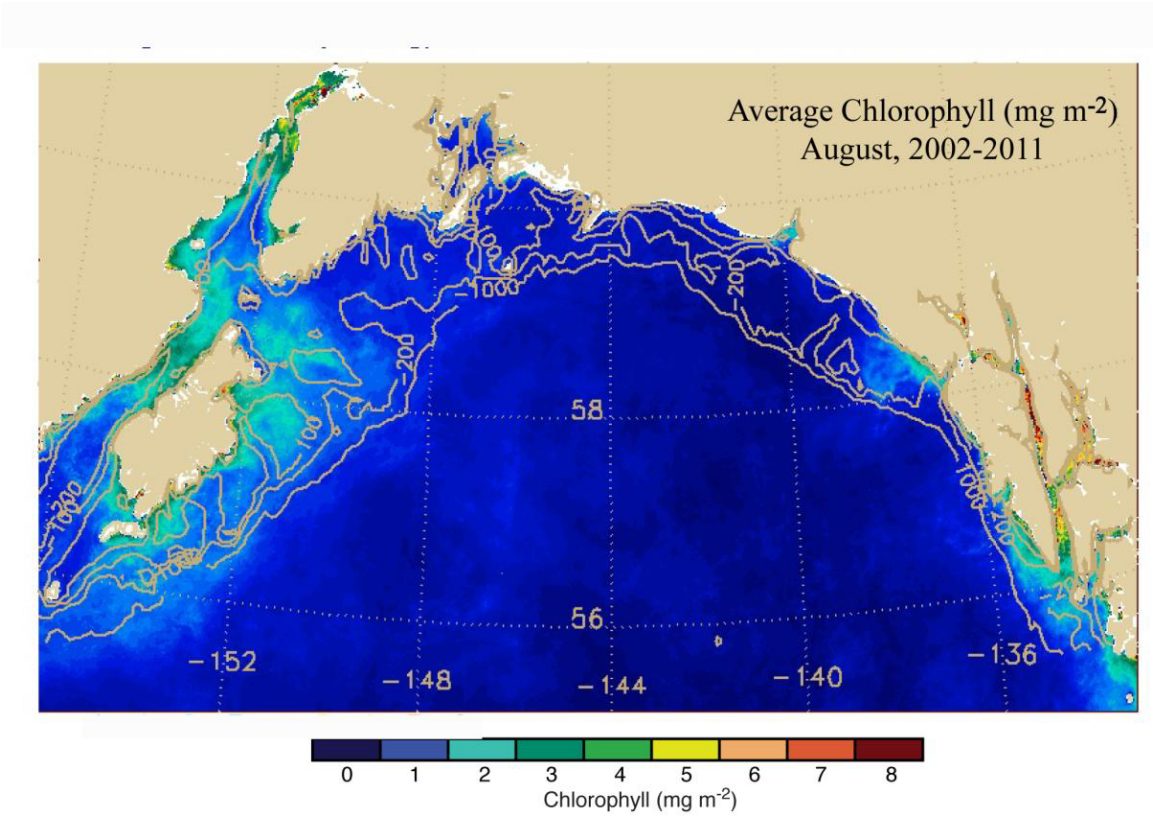

Figure 14. SeaWiFS chlorophyll averaged between June 1 and August 31 for 1998-2002 showing the high, sustained productivity that takes place around Kodiak Island.

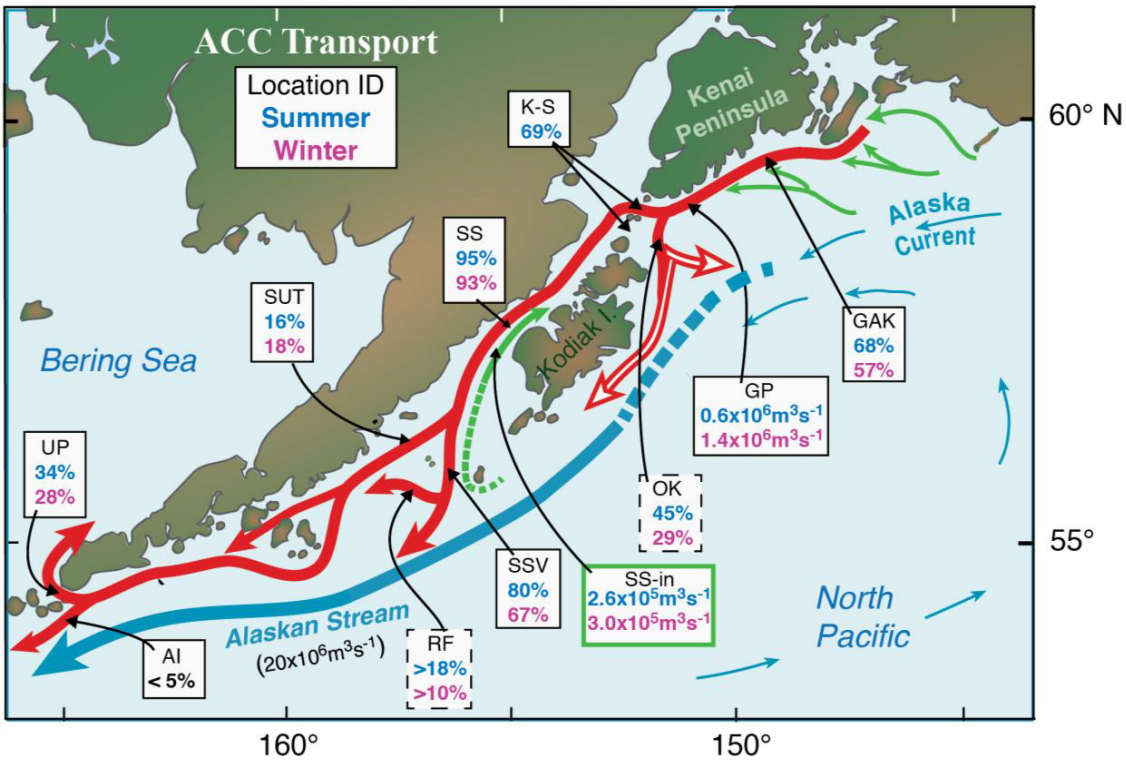

Figure 15. Composite map of transport in the various banches of the ACC from Kayak Island to the Aleutian Islands. The hollow arrows are extrapolated pathways of the ACC. The thin green lines indicate likely contributions to the ACC in the east and measured upstream flow in Shelikof Strait. The highest mean transport was measured at Gore Point. The other squares indicate the percent of transport at Gore Point (GP) that occurs on each branch. The magnitude of inflow in Shelikof Strait is also given (green box). The transports at the exit to Shelikof Strait (SS), Kennedy-Stevenson Entrances (K-S), south side of Kodiak Archipeligo (OK) and Seward (GAK) are from this paper. The estimate of transport between Sutwik and the Semidi Islands (Sut) and between the Semidi Islands and Chirikof Islands (SSV) are from Schumacher et al. (1989). The flow through Unimak Pass (UP) is from Stabeno et al. (2016, in press) and Aleutian Islands (AI) continuation is estimated from Stabeno et al. (2005).